THE EFFECTS OF DIAGENESIS ON LITHIUM ISOTOPE RATIOS OF SHALLOW MARINE CARBONATES

MATHIEU DELLINGER[1], A. JOSHUA WEST[2], NOAH J. PLANAVSKY[3], DALTON S. HARDISTY[4], BENJAMIN C. GILL[5], BORIANA KALDERON-ASAEL[3], DAN ASAEL[3], THOMAS CROISSANT[1], PETER K. SWART[6]

ABSTRACT. In this study, we present new data on the δ^7Li values and Li/(Ca+Mg) ratios of carbonate cores from the Great Bahama Bank (Clino, Unda), a deep water core off of the bank top (ODP Leg 166 Site 1007), and the coralline Key Largo Limestone. We use these samples to evaluate the influence of meteoric diagenesis, marine burial diagenesis, and dolomitization on the Li isotope system in carbonates. We find that recrystallization of aragonite to low-Mg calcite in the presence of meteoric fluids results in a systematic decrease of the Li/(Ca+Mg) ratio in Clino, Unda and Key Largo samples, due to the lower Li/(Ca+Mg) ratio in meteoric fluids compared to seawater. For Li isotopes, we observe that the δ^7Li of meteorically altered low-Mg calcite is +22.0±3.8‰ (n=28, 1σ), which is coincidentally similar to the original aragonite-rich sediments (+22±1‰ in the Bahamas, +18±1‰ in Key Largo), but with a larger variability (from +15 to +27‰). We interpret these features as reflecting the overprinting of primary Li during meteoric alteration with a highly variable isotope signature that may be controlled by a combination of local porewater and/or global climatic conditions; in either case, meteoric diagenesis produces isotopic signatures that are unrelated to seawater composition. In contrast, marine burial diagenesis and dolomitization of Clino and Unda sediments under "fluid-buffered" conditions result in Li isotope composition that is similar (+30.2±1.5‰, n=36, 1σ) to modern seawater (+31‰). For Site 1007, the δ^7Li values range between +23‰ and +31‰. We interpret this range as reflecting a combination of varying diagenesis style (fluid to sediment-buffered) and varying contribution of calcite derived from pelagic sediments, with distinct isotopic composition due to primary mineralogy. Altogether, our results show that diagenesis does not invalidate the use of bulk carbonates for deriving Li isotope paleo-records, but the reliability of past carbonates as recorders of seawater δ^7Li values will depend on carefully characterizing their diagenetic history.

Keywords: Bahamas, Diagenesis, Lithium isotopes, Lithium incorporation, Dolomite

[1] Department of Geography, Durham University, South Road, Durham, DH1 3LE, United Kingdom
[2] Department of Earth Sciences, University of Southern California, 3651 Trousdale Pkwy, Los Angeles, CA 90089, USA
[3] Department of Geology and Geophysics, Yale University, New Haven, CT 06511, USA
[4] Department of Earth and Environmental Sciences, Michigan State University, 288 Farm Lane, East Lansing, MI 48824, USA
[5] Department of Geosciences, Virginia Polytechnic and State University, Blacksburg, VA, USA
[6] Department of Marine Geosciences, Rosenstiel School of Marine and Atmospheric Science, University of Miami, Miami, FL 33149, USA
Corresponding author: mathieu.dellinger@durham.ac.uk

1. Introduction

The lithium (Li) isotope composition (δ^7Li) of ancient carbonate rocks has emerged as a promising proxy for tracing past weathering and hydrothermal processes (Misra and Froelich, 2012; Pogge von Strandmann et al., 2013; Hathorne and James, 2006). Lithium has two stable isotopes, ^{7}Li and ^{6}Li, that are strongly fractionated during water-rock interaction, with the lighter isotope, ^{6}Li, usually preferentially incorporated into secondary minerals relative to the heavy isotope, ^{7}Li (Chan et al., 1992; Huh et al., 1998). Interest in applying this proxy has led to the publication of Li isotope records from past carbonate, using specific organisms like foraminifera (Misra and Froelich, 2012), brachiopods (Pogge von Strandmann et al., 2017) and belemnites (Ullmann et al., 2013), as well as bulk shallow- and deep-water carbonates (Lechler et al., 2015; Pogge von Strandmann et al., 2013; 2019). These studies have documented significant Li isotope variations during geologically short warming (Lechler et al., 2015; Pogge von Strandmann et al., 2013) and cooling events (Pogge von Strandmann et al., 2017) as well as long-term

gradual changes of the δ^7Li value of the ocean (Misra and Froelich, 2012). These changes have been interpreted as resulting predominately from variations in continental and reverse weathering over time, providing new insights into the evolution and operation of the long-term global carbon cycle. However, the reliability of the Li isotope proxy in carbonate depends upon the extent to which the initial δ^7Li value of seawater is influenced by isotope effects during carbonate precipitation (e.g. mineralogy, vital effects, ocean environmental parameters) and subsequently by diagenetic processes. Several studies have documented Li isotope effects during carbonate formation, both for abiogenic (Marriott et al., 2004a,b; Taylor et al., 2019) as well as biogenic carbonates (Rollion-bard et al., 2009; Hathorne and James 2006; Misra and Froelich, 2012; Dellinger et al., 2018). Yet so far, very little is known about the behavior of Li isotopes during diagenesis—despite some evidence for potentially significant post-depositional alteration of primary values (Ullman et al., 2013).

There are a wide range of diagenetic processes that can influence the geochemical composition of carbonates (Brand and Veizer, 1980; Lohmann, 1988; Swart, 2015; Hood et al., 2018). Meteoric diagenesis occurs via interaction between meteoric or groundwater fluids and carbonates, primarily when carbonates are exposed to the atmosphere during seawater low-stands or by tectonic uplift (James and Choquette, 1984; Lohmann, 1988). Meteoric fluids generally have low to neutral pH and are undersaturated with respect to carbonate phases. These fluids dissolve primarily aragonite and high-Mg calcite (HMC) which are the most soluble phases, eventually reach calcite saturation, and then precipitate low-Mg calcite (LMC) that is stable under meteoric conditions (Lohmann, 1988; Swart, 2015). The composition of the meteoric fluids is influenced by chemical processes within the open systems of the soil vadose zones (Moore and Wade, 2013a), and therefore these fluids may have different δ^7Li value and Li/Ca ratios relative to the original composition of carbonates (Pogge von Strandmann et al., 2017).

In addition to meteoric diagenesis, marine burial diagenesis can lead to the mineralogical transformation of primary carbonate, and, depending in part of fluid-to-rock ratios, can alter the primary chemical signature of carbonates in the process (Banner and Hanson, 1990). This type of diagenesis takes place in the marine environment and can occur below the meteoric diagenesis zone. In this process, primary aragonitic carbonates are dissolved by marine pore fluids, and secondary low-Mg calcite and/or dolomite are precipitated (Moore and Wade, 2013b). Marine pore fluids usually have seawater-like composition but can also be influenced by reactions with silicates if present, or by mixing with fresh groundwater fluids. The style of marine burial diagenesis is controlled by the permeability of the sediments and the fluid advection rate (Fantle et al., 2010; Higgins et al., 2018; Melim et al., 2001). When diagenesis occurs in a closed system (e.g. for low rates of fluid advection and low permeability), the composition of the diagenetic carbonates is primarily determined by the original composition of the sediments ("sediment-buffered" diagenesis; Higgins et al., 2018). For high fluid flow rates and permeability, open-system diagenesis can lead to the precipitation of diagenetic carbonate with composition reflecting that of the fluid rather than the original carbonate ("fluid-buffered" diagenesis).

The goal of this study is to investigate how the Li isotope composition of marine carbonates, and in particular shallow water platform carbonates that are abundant in the geological record, are affected by both meteoric and marine burial diagenesis. We begin with quantitative theoretical consideration, including discussion on published experimentally-derived partition coefficient values and isotopic fractionation factors in order to evaluate the extent to which we expect δ^7Li values and Li/Ca ratios to be affected by diagenesis under different conditions (Section 2). Then, in Sections 3-7, we present and discuss new measurements of the Li isotope composition and Li/(Ca+Mg) ratios of carbonate sediments from the Clino, Unda and 1007 cores from the Great Bahama Banks (GBB), along with altered corals from the Key Largo Limestone. Finally, in Section 8, we use these data to assess the behavior of Li isotopes during diagenesis and provide guidelines for interpreting the δ^7Li of ancient carbonates. These results have important implications for understanding the past Li isotope record of platform carbonate sediments.

2. Theoretical influence of diagenesis on δ^7Li and Li/Ca ratios

Prior work on carbonate diagenesis informs our approach to studying the effects on lithium specifically. In a series of seminal papers, Brand and Veizer identified general controls on the isotopic and trace element composition of diagenetic carbonates (Brand and Veizer, 1980, 1981). In the context of Li, these are: i) the partitioning coefficient of Li between secondary carbonate and fluids (Kd^{Li}) and the Li isotope fractionation factor between the diagenetic carbonate and the fluid ($\Delta^{Li}_{carb\text{-}fluid}$), ii) the composition of the initial diagenetic fluid, both

elemental and isotopic, i.e., $(Li/Ca)_{fluid\ 0}$ and $\delta^7Li_{fluid\ 0}$, respectively, iii) the elemental and isotopic composition of the original solid, $(Li/Ca)_{prim}$ and δ^7Li_{prim}, and iv) the extent to which diagenesis is fluid-buffered (open system) or sediment-buffered (closed system). In the following sections, we consider each of these factors in sequence.

In sections 2.1-2.3, we follow the approach of Brand and Veizer (1980) and summarize what is known about key controls from field and experimental data. We then use this foundational understanding about how Li and its isotopes behave during water-carbonate interactions to make general predictions for how Li/Ca and δ^7Li in carbonates may be affected by diagenesis, in section 2.4. In section 2.5, we turn to consider the role of fluid-buffered vs. sediment-buffered diagenetic conditions. The actual composition of the diagenetic carbonates will depend on the extent of fluid-rock interaction, and we adopt a mass balance model to quantify this effect (Banner and Hanson, 1990; Ahm et al., 2018). This model also allows us to compare the predicted behavior of Li with other carbonate geochemical signatures (in section 2.6). Taken together, this background information sets the foundation for our study of Li isotope compositions in Bahamian carbonates. Because most experimental data for LMC have been reported in terms of Li/Ca, we use this notation here, but later in the manuscript we use the Li/(Ca+Mg) ratio value in order to avoid biases when comparing ratios between LMC and dolomites (Li/Ca ~ Li/(Ca+Mg) for LMC, but not for dolomite). Also, because diagenetic influence is element-specific, in the following, we refer to fluid- or sediment-buffered as being with respect to Li in the carbonate, unless otherwise specified.

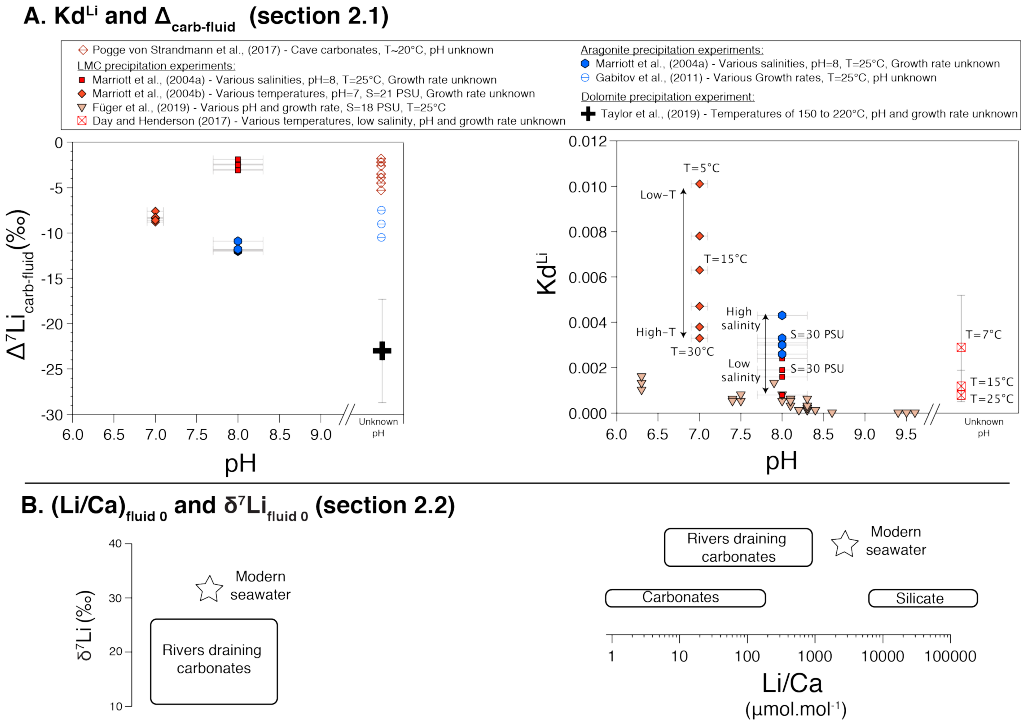

Figure 1. Partitioning of Li and fractionation of its isotopes during carbonate formation, and typical fluid compositions. (A) Summary of published experimental Li isotope fractionation factors ($\Delta^7Li_{carb\text{-}fluid}$) and partition coefficients (Kd^{Li}) between carbonates and fluid as a function of pH. (B) δ^7Li and Li/Ca composition of rivers draining carbonates (Kisakurek et al., 2005, Millot et al., 2010 and supplementary data table), seawater (Misra and Froelich, 2012) and range of Li/Ca in carbonate and silicate rocks.

2.1. Li Partition coefficient and fractionation factor between carbonates and fluid: Kd^{Li} and $\Delta^7Li_{carb\text{-}fluid}$

A handful of experimental studies (Day and Henderson, 2013; Füger et al., 2019; Marriott et al., 2004a; Marriott et al., 2004b) have determined the apparent partition coefficient of Li (Kd^{Li}) between fluids and both abiogenic LMC and aragonite (see compilation in Fig. 1A). Overall, the total range of possible Kd^{Li} values for typical natural waters is low (Kd^{Li} of 10^{-4} to 10^{-2}), which means that Li is strongly partitioned in favor of the fluid rather than calcite during inorganic LMC precipitation. While there is uncertainty in terms of what controls the Kd^{Li} value, the available data suggest that the Kd^{Li} of LMC decreases with increasing temperature and pH but increases with increasing salinity and growth rate. Importantly, it appears that for a similar set of typical marine

conditions, the Kd^{Li} of inorganic aragonite is higher (Kd^{Li} ~ 0.0025 to 0.0035) than for inorganic LMC (Kd^{Li} ~ 0.0005 to 0.0020).

Experimental studies have shown that the Li isotope fractionation factor for aragonite ($\Delta^7Li_{Aragonite\text{-}fluid}$) ranges from –12 to –8‰ (Fig. 1A) and may be controlled by crystal growth rate (Marriott et al., 2004b; Gabitov et al., 2011). In comparison, the Li isotope fractionation factor for LMC is lower than for aragonite ($\Delta^7Li_{LMC\text{-}fluid}$ = –8 to –1‰) and unlike the Kd^{Li}, is not significantly influenced by temperature or salinity (Marriott et al., 2004a; Marriott et al., 2004b). It has been suggested (Coogan et al., 2016) that there might be a strong control by pH as the $\Delta^7Li_{LMC\text{-}fluid}$ determined at pH = 8 ($\Delta^7Li_{LMC\text{-}fluid}$ = –2.5±1.5‰) is significantly higher relative to that at pH = 7 ($\Delta^7Li_{LMC\text{-}fluid}$ = –8±1‰). Similarly, an influence of pH on the δ^7Li of biogenic LMC such as benthic foraminiferal tests has also been proposed (Roberts et al., 2018). A speleothem study by Pogge von Strandmann et al. (2017) measured a field-based fractionation factor of $\Delta^7Li_{LMC\text{-}fluid}$ = –3±2‰, in good agreement with experimental results at pH = 8 (Marriott et al., 2004a). For dolomite, a recent study reported a Li isotope fractionation factor between dolomites and fluids ($\Delta^7Li_{Dolomite\text{-}fluid}$ = –23±5.8‰ at 25°C) much larger than $\Delta^7Li_{Aragonite\text{-}fluid}$ and $\Delta^7Li_{LMC\text{-}fluid}$ (Taylor et al., 2019), though this value is an extrapolation from experiments done at high temperature (150°C to 220°C). While $\Delta^7Li_{Dolomite\text{-}fluid}$ remains least well constrained, overall it appears that there is a strong mineralogical control on the Li isotope fractionation factor between inorganic carbonates and fluids.

2.2. Composition of the diagenetic fluid: $(Li/Ca)_{fluid\ 0}$ and $\delta^7Li_{fluid\ 0}$

Given that we expect the Li in carbonates to be influenced by the composition of diagenetic fluids in many settings, understanding the controls on fluid composition will be important for interpreting carbonate isotopic signatures. Where diagenesis takes place through interaction with meteoric fluids (i.e., "meteoric diagenesis"), we expect the fluid composition to reflect reactions in overlying weathering zones and thus have a δ^7Li value in between that of the original carbonate (typically δ^7Li in the range of ~15-30‰ in the present-day; Misra and Froelich, 2012; Pogge von Strandmann et al., 2013 and 2017) and weathering of other phases, including detrital and dust sources (typically ~0-5‰, characteristic of silicate rocks; Sauzéat et al., 2015). Since carbonates contain much less Li (0-5 ppm, Li/Ca in the range of 1-200 $\mu mol.mol^{-1}$) than silicates (5-100 ppm, Li/Ca of 8000-200000 $\mu mol.mol^{-1}$; Dellinger et al., 2018; Sauzéat et al., 2015; Teng et al., 2004), even small amounts of silicates can dominate the dissolved Li budget and consequently control the isotope composition of fluids (as seen in karst settings by Pogge von Strandmann et al., 2017). The range of Li/Ca and δ^7Li of rivers draining carbonate terranes (i.e. an analogue to diagenetic meteoric fluids) are respectively 7-700 $\mu mol.mol^{-1}$ and +10 to +26‰ (Fig. 1B). In the case of diagenesis taking place through interaction with marine porewaters (i.e., "marine burial diagenesis"), fluid δ^7Li may be close to seawater isotope composition, perhaps modified by diffusion or reaction with carbonates or other phases in pore waters (Scholz et al., 2010).

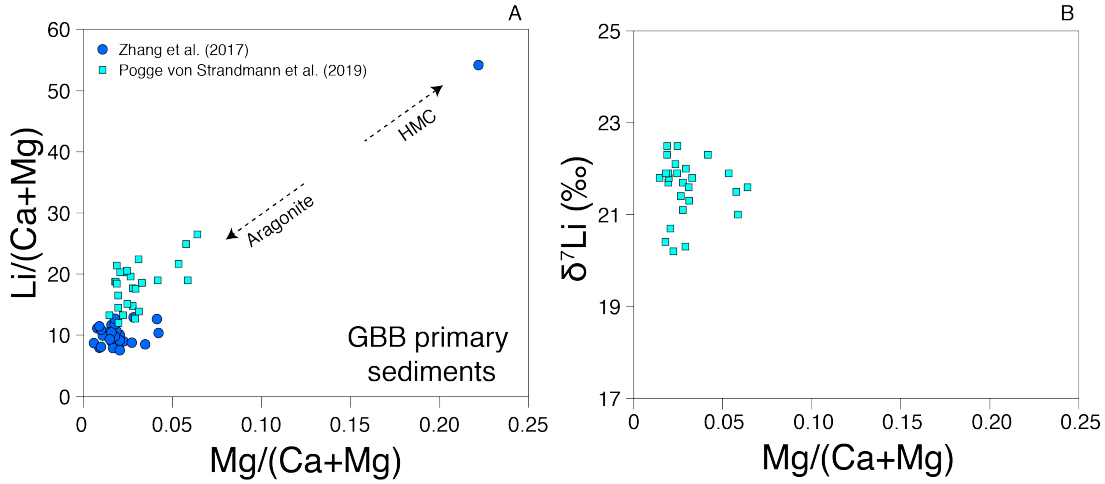

Figure 2. Composition of unaltered Great Bahama Banks sediments. (A) Li/(Ca+Mg) ratio (in $\mu mol.mol^{-1}$) and (B) δ^7Li as a function of the Mg/(Ca+Mg) ratio (in $mol.mol^{-1}$). Data are from Zhang et al. (2017) and Pogge von Strandmann et al. (2019). Note that Zhang et al. (2017) did not report isotopic data for their samples.

2.3. Composition of the original solid

In the modern oceans, we would expect primary abiotic aragonite to have δ^7Li ~ 19-24‰ and Li/Ca ~ 7-12 μmol.mol^{-1}, based on modern seawater δ^7Li of 31 ‰ and Li/Ca of 2500 μmol.mol^{-1}, and the partition coefficients and fractionation factors described in section 2.1, above. However, abiotic primary aragonite is scarce in the modern ocean, and even when non-skeletal carbonate forms (e.g., as pelloids and ooids), it is often associated with fecal pellets, fossil fragments, and other material (Schlager, 2005). Moreover, platform and peri-platform carbonates can include abundant biogenic carbonates, and these have very wide-ranging Li compositions partly but not only determined by their mineralogy (Dellinger et al., 2018). Despite all of this potential complexity, measurements of bulk modern carbonates from the GBB (Zhang et al., 2017; Pogge von Strandmann et al., 2019) paint a picture that is relatively simple and consistent with the experimental partitioning coefficients and fractionation factors.

Present-day GBB platform carbonates (as described by Reijmer et al., 2009) are composed mostly of non-skeletal (peloids and ooids) aragonite (between 60 and 100%, average of 93%) with a minor component of HMC (average of 7%) and almost no LMC (<1%). The Li/Ca ratio of modern GBB sediments from Zhang et al. (2017) ranges from 8 to 12 μmol.mol^{-1} (average 10.2±1.6 μmol.mol^{-1}), while the Li/Ca ratios reported by Pogge von Strandmann et al. (2019) are higher and range from 12 to 28 μmol.mol^{-1} (average 18.6 ± 4 μmol.mol^{-1}). These differences can be ascribed to different concentrations of HMC; indeed, the relationship between Li/Ca and Mg/Ca ratios in these samples reveals systematic trends that we interpret as mixing between aragonite and HMC (Fig. 2A). This arises because the Li/Ca ratio of HMC is generally much higher than the Li/Ca ratio of aragonite (Darrenougue et al., 2014; Dellinger et al., 2018). Interestingly, the mean HMC proportion in the Zhang et al. (2017) sample set (17%) is higher than the average HMC content in GBB sediments (7%) determined by Reijmer et al. (2009) from a much larger number of samples, so even the Zhang et al. (2017) data reflects a mixed composition that does not, on its own, represent bulk unaltered GBB sediments. The aragonite-rich end-member defined by the correlation in Fig. 2A has a Li/Ca of 9±1 μmol.mol^{-1}, compatible with the expected composition of abiotic aragonite precipitating from present-day seawater (7.5±1.0 μmol.mol^{-1}), as deduced from the experimental Kd^{Li} values discussed above. We see this Li/Ca value as representative of primary unaltered aragonite.

The δ^7Li of GBB sediments from Pogge von Strandmann et al. (2019) is ~22±1‰ and shows no relationship with Mg/Ca (Fig. 2B), suggesting that the δ^7Li of HMC in the Bahamas is not significantly different from aragonite. Hence, we can consider the δ^7Li of GBB sediments from Pogge von Strandmann et al. (2019) as representative of GBB primary unaltered sediments. This δ^7Li value is within the range (19-24‰) expected for precipitation from seawater assuming the experimentally-determined inorganic aragonite fractionation factor.

We have focused here on primary carbonate compositions from the GBB, since modern bulk data are available. Importantly, the diagenetically altered samples we have studied are also from this region (see Section 3), so we can be confident in assigning the unaltered end-member for our samples on the basis of these data. Additional work on modern bulk carbonates from other settings would help to establish whether the primary aragonite compositions inferred here are globally applicable. In any case, we adopt these compositions for the general consideration that follows.

2.4. Expected effects of diagenesis on bulk carbonate δ^7Li_{dCarb} and $(Li/Ca)_{dCarb}$ ratios

Based on the experimental data on partition coefficients and fractionation factors from section 2.1, together with expectations of fluid and original solid compositions from sections 2.2 and 2.3, we can predict the change in δ^7Li and Li/Ca during diagenetic conversion of aragonite to LMC or dolomite in the context of the shallow marine carbonates, such as those in the Bahamas. Here we focus on fluid-buffered diagenesis, and we consider the effect of sediment-buffered conditions in the next section (section 2.5). For fluid-buffered diagenesis, the Li/Ca ratio of diagenetic carbonates $(Li/Ca)_{dCarb}$ can be expressed as:

$$\left(\frac{Li}{Ca}\right)_{dCarb}^{fluid-buffered} = Kd^{Li} \times \left(\frac{Li}{Ca}\right)_{fluid\ 0} \quad (1)$$

where $(Li/Ca)_{fluid\ 0}$ is the Li/Ca ratio of the initial advecting fluid and Kd^{Li} is the apparent partition coefficient of Li between carbonate and fluid ($Kd^{Li} = (Li/Ca)_{carb} / (Li/Ca)_{fluid}$). Similarly, the δ^7Li_{dCarb} of fluid-buffered carbonates can be expressed as:

$$\delta^7Li_{dCarb}^{fluid-buffered} = \delta^7Li_{fluid\ 0} + \Delta^7Li_{carb-fluid} \qquad (2)$$

where $(\delta^7Li)_{fluid\ 0}$ is the δ^7Li value of the initial advecting fluid and $\Delta^7Li_{carb\text{-}fluid}$ is the Li isotopic fractionation factor between the carbonate and fluid ($\Delta^7Li_{carb\text{-}fluid} \sim 1000\ \ln(\alpha^{Li}_{carb\text{-}fluid})$).

So, what does all of this mean, considering what we know about the respective partition coefficients and fractionation factors (section 2.1)? Predicted changes in composition as a result of transformation of aragonite to LMC and dolomite are shown in Fig. 3A. The inorganic Kd^{Li} of LMC is lower than that for inorganic or biogenic aragonite (Hathorne et al., 2013; Marriott et al., 2004a, 2004b), so transformation of aragonite to calcite should result in lowering of the Li/Ca of limestones (Fig. 3A) if the fluid composition and temperature are the same, as expected for marine pore waters. Meanwhile, we expect that δ^7Li would increase, because of the smaller fractionation factor into calcite than aragonite. Altogether, for typical marine pH (7.5 to 8.5) and Bahamian temperature and salinity, the Li/Ca of fluid-buffered diagenetic LMC should be ~1-6 µmol.mol^{-1} and δ^7Li of +26 to +30‰ (marine LMC region in Fig. 3A). If the diagenetic transformation of aragonite to calcite takes place at lower temperatures (e.g. T < 10°C) or lower pH (e.g. pH < 7.5) than aragonite formation, the expected compositions might differ both in terms of elemental and isotopic ratios (illustrated by dashed arrows in Fig. 3A). Specifically, the Kd^{Li} of calcite increases with decreasing temperature (Marriott et al., 2004a,b) and decreasing pH (Füger et al., 2019), so lower T and lower pH both may yield Li/Ca ratio of LMC higher than primary inorganic aragonite (> 10 µmol.mol^{-1}). Temperature of diagenetic reactions is not likely to affect δ^7Li, but pH might, and diagenesis at pH ~ 7.5 might produce δ^7Li < 23‰ according to experimental $\Delta^7Li_{carb\text{-}fluid}$ at pH=7 (Marriott et al., 2004a).

For the formation of dolomite during marine diagenesis, the Li isotope fractionation inferred from experiments (Taylor et al., 2019) predicts diagenetic dolomite δ^7Li significantly lower than δ^7Li values for aragonite, LMC and seawater (dolomite region in Fig. 3A). However, if the fractionation factor for dolomite is more similar to that for calcite, we would expect higher δ^7Li values than shown in Fig. 3A. In the absence of any experimental or other constraints on the Kd^{Li} for dolomite, it is not possible to make any prediction on the Li/(Ca+Mg) for dolomites.

For meteoric diagenesis, we expect an even larger decrease in carbonate Li/Ca (< 2 µmol.mol^{-1}) relative to primary aragonite than for marine diagenesis, because the Li/Ca of meteoric fluids (e.g., rivers) tends to be lower than that of seawater-derived carbonates (Fig. 1B), and because the Li partition coefficient (Kd^{Li}) is lower in inorganic LMC compared to either primary aragonite or biogenic calcite (Fig. 1A). Considering the range of δ^7Li in modern rivers draining limestones (Fig. 1B), we expect a δ^7Li in meteoric LMC in the range of +5 to +25‰, lower than present-day oceanic δ^7Li value (meteoric LMC region in Fig. 3A).

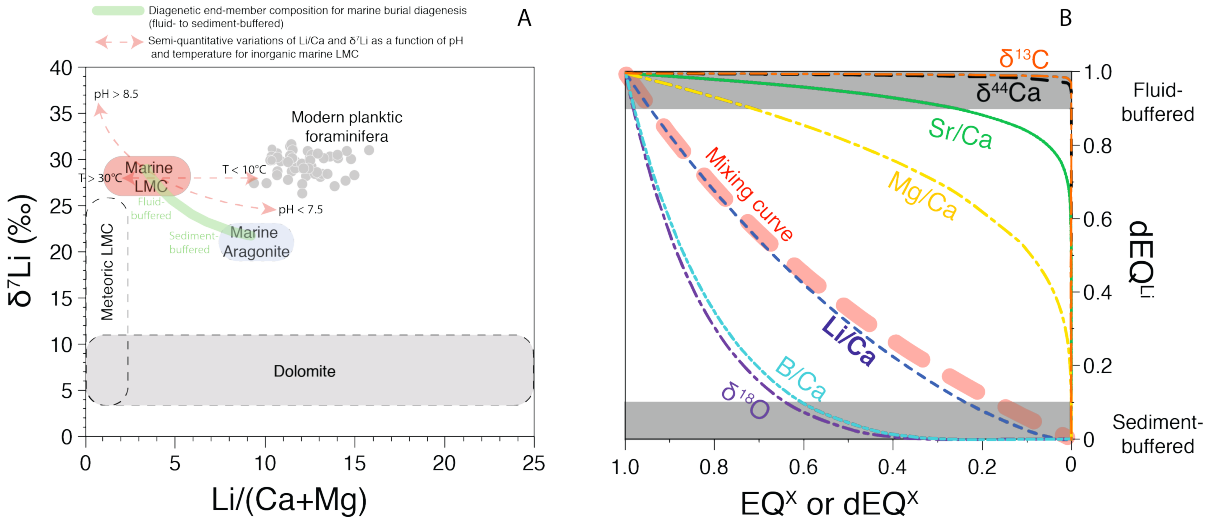

Figure 3. (A) Expected effects of diagenesis on Li isotopes and Li/(Ca+Mg) ratios (in μmol.mol^{-1}). The composition of marine aragonite is from Section 2.3. The other compositions (e.g., marine LMC, meteoric LMC) are based on fluid-buffered diagenesis, following Eqs. 1 and 2. The green curve showing the expected trajectory between fluid- and sediment-buffered conditions is determined using the diagenesis model equations from Appendix 1. Note that we shift here and in the remainder of this paper to using Li/(Ca+Mg), rather than Li/Ca as in Fig. 1, in order to compare the elemental compositions of calcite and dolomite. (B) Carbonate compositions expected to result from alteration of aragonite to LMC in reaction with seawater fluid with modern composition for several geochemical proxies, calculated using the diagenesis model equations from Appendix 1. The black horizontal bars correspond to fluid-buffered ($dEQ^{Li} > 0.9$) and sediment-buffered compositions ($dEQ^{Li} < 0.1$) in regard to Li isotopes. The red dotted curve corresponds to the mixture between fluid-buffered (for all elements, EQ^X and $dEQ^X > 0.9$) and sediment-buffered LMC (EQ^X and $dEQ^X < 0.1$).

2.5. The effect of fluid vs. sediment buffered conditions

Thus far, we have considered predictions for fluid-buffered conditions. However, as noted above, actual diagenetic transformations occur across a range of conditions that vary from fluid- to sediment-buffered, and these conditions can strongly affect the composition of carbonate that forms (Brand and Veizer, 1980). The composition of carbonate precipitated in fluid-buffered conditions has been described in section 2.4, above. For carbonate precipitation in sediment-buffered conditions, the geochemical and isotopic composition of diagenetic carbonates will be unchanged relative to the primary aragonite carbonates, so $(Li/Ca)_{dcarb} = (Li/Ca)_{prim}$ and $\delta^7Li_{dcarb} = \delta^7Li_{prim}$. In between these two diagenetic end-members, the composition of the diagenetic carbonates has intermediate values depending on the extent of fluid-rock interaction (Banner and Hanson, 1990). To capture the range of predicted compositions, we also need to account for the evolution of fluid chemistry with the extent of reaction (Fantle et al., 2010). We can do this by following recent work (Ahm et al., 2018) in combining mass-balance calculations (Banner and Hanson, 1990) with 1-D reactive-transport calculations corresponding to a reaction between a downward advecting fluid and sediments. In this way, we can calculate the range of expected composition for diagenetic carbonates depending on specific chemical and physical parameters (e.g. depth of diagenetic reactions, fluid advection rates, reaction rates), and using the background information for Li established in sections 2.1-2.3. In Appendix (A1), we provide a full expression for the diagenetic effects on LMC based on a 1-D mass-balance reactive-transport framework (Ahm et al., 2018; Pogge von Strandmann et al., 2014). Here and in Fig. 3, we report a summary of the predictions for marine diagenesis.

The predicted effect of shifting from sediment- to fluid-buffered conditions is relatively straightforward: the compositional range of predicted diagenetic LMC (sediment-buffered to fluid-buffered) displays a negative curve in δ^7Li-Li/(Ca+Mg) space (green curve in Fig. 3A). We expect diagenetic carbonates to fall along a similar trajectory, depending on the specific conditions. It is readily apparent from this analysis that there is a potentially large range of carbonate compositions, both in terms of δ^7Li and Li/(Ca+Mg), that can result depending on whether reactions are fluid- or sediment-buffered (e.g., ~10‰ range in δ^7Li along this trajectory in Fig. 3A). Thus, accurately interpreting the Li isotope composition of marine carbonates will depend on identifying the diagenetic conditions – not just whether the carbonates are altered diagenetically, and not just whether that was by meteoric or marine fluids, but also the extent to which marine diagenesis was fluid or sediment buffered.

2.6. Contextual information from other geochemical proxies in diagenetic carbonates

It is usually a challenge to know the extent of fluid advection (i.e. the cumulative fluid-rock ratio) through ancient carbonate sediments, as would be needed to assess whether the diagenetic carbonate composition is fluid or sediment-buffered. But it may still be possible to constrain the degree of diagenetic resetting of ancient carbonate rocks by comparing between chemical proxies (e.g. Sr/Ca, Mg/Ca, $\delta^{13}C$, $\delta^{18}O$, $\delta^{44}Ca$ and others; Brand and Veizer 1980). Because the original signature (prior to diagenesis) of mineralogical phases of different proxies can vary in space and time, we follow Banner and Hanson (1990) and define the EQ^X parameter which corresponds to the extent to which the concentration of the element X in the diagenetic product is fluid-buffered ($EQ^X > 0.9$) or sediment-buffered ($EQ^X < 0.1$):

$$EQ^X = \frac{[X]_{dCarb} - [X]_{prim}}{[X]_{fluid-buffered} - [X]_{prim}} \qquad (3)$$

Similarly, we can define the dEQ^X for isotope ratios ($\delta^Y X$):

$$dEQ^X = \frac{\delta^Y X_{\,dCarb} - \delta^Y X_{\,prim}}{\delta^Y X_{\,fluid-buffered} - \delta^Y X_{\,prim}} \qquad (4)$$

with $[X]_{dCarb}$, $[X]_{prim}$, $[X]_{fluid\text{-}buffered}$ and $\delta^Y X_{dCarb}$, $\delta^Y X_{prim}$, $\delta^Y X_{fluid\text{-}buffered}$ respectively the concentration and isotope composition of the element X in diagenetic, primary and fluid-buffered carbonates. The advantage of this notation is that, for a given fluid composition and fluid-rock ratio, the EQ^X value for any element is independent of the concentration in the initial solid and fluid. Different chemical elements will have distinct EQ values as the latter is then only controlled by the partition coefficient of a given element (Banner and Hanson, 1990; Jacobsen and Kaufman, 1999). Thus, comparison between elements provides a method to estimate the degree of fluid and sediment buffered diagenesis of ancient limestones.

An example of a diagenetic end-member calculation for several geochemical proxies is shown for diagenetic transformation of aragonite to LMC in modern-type seawater fluid in Fig. 3B (using equations from appendix A1, and modern seawater compositions for the fluids). We observe that for a given set of conditions, Li/Ca ratios and δ^7Li values have lower EQ and dEQ values than B/Ca and oxygen isotopes and higher values than Mg/Ca, Sr/Ca, calcium and carbon isotopes. This analysis is important for several reasons. First, evidence for preservation of the δ^{18}O or B/Ca primary composition in ancient carbonates (i.e. sediment buffered composition for δ^{18}O and B, EQ^O and $EQ^B < 0.1$) implies that the Li/Ca and δ^7Li are also likely to be sediment-buffered ($dEQ^{Li} \sim 0$). Second, evidence that Sr, C, Mg or Ca have fluid-buffered compositions ($EQ \sim 1$) would indicate that Li will also be reset to fluid values by diagenetic reactions ($dEQ^{Li} \sim 1$). Third, the diagenetic LMC end-members define specific trends in cross-plots between δ^7Li and other geochemical proxies (Fig. 3B), and these trends can be used to discriminate fluid-buffered and sediment-buffered diagenesis. Fourth, as shown for other proxies (Ahm et al., 2018), a fluid-buffered Li isotope composition ($dEQ^{Li} \sim 1$) corresponds a large range of Sr/Ca, δ^{13}C and δ^{44}Ca values. Fifth, diagenetic trends are distinct from mixing trends (of diagenetic end-members, except in the δ^7Li – Li/Ca space) making it possible to discriminate diagenetic paths relative to mineral mixing (Fig. 3B). Note that these results might vary for a different set of parameter values (e.g., different fluid composition, fractionation factor, or partition coefficient value), but it is beyond the scope of this study to explore the total range of possible values of Li/Ca, δ^7Li, and other proxies resulting from diagenetic processes.

The key point is that theoretical calculations informed by experimental data on Li partitioning and isotope fractionation allow us to make predictions about Li isotope effects under different diagenetic conditions. These suggest potentially significant diagenetic effects that vary as a function of diagenetic process and environmental conditions, and that we may be able to tease apart the specific conditions by comparing to other element and isotope systems. These predictions set the stage for our analysis of Bahamas carbonate samples.

3. Samples

In this study, we have analyzed shallow water platform carbonates from the Florida Keys and the Great Bahamas Bank, specifically from the Clino, Unda, and ODP 1007 cores (Fig. 4). The locations and number of samples measured in this study are indicated in Table (1). These samples represent primary GBB carbonates (as described in section 2.3) that have been altered by different types of diagenesis (meteoric and marine) and in environments characterized by different fluid advection rates (Caspard et al., 2004; Melim et al., 1995; Swart and Oehlert, 2018). One additional difference is that the modern to mid-Pliocene sediments found within Clino and Unda are predominantly platform facies with minor pelagic components (foraminifera and coccoliths), while the sediments from the peri-platform facies from core 1007 contain a higher proportion of pelagic material (and thus some contribution from primary low-Mg calcite, with distinct Li systematics, e.g., see Fig. 4).

The samples we have analyzed correspond to those used in previous studies of diagenetic alterations to carbonate proxies, specifically for I/(Ca+Mg) (Hardisty et al., 2017), δ^{238}U (Chen et al., 2018a), REEs (Liu et al., 2019), and carbonate-associated sulfate for Key Largo samples (Gill et al., 2008). The samples have also been previously characterized for δ^{13}C, δ^{18}O, and mineralogy (Hardisty et al., 2017; Gill et al., 2008; Swart and Eberli, 2005). In addition, δ^{44}Ca, δ^{26}Mg, and δ^{11}B have been measured on the same Bahaman cores (although not the exact samples used here) as part of other previous studies (Higgins et al., 2018; Stewart et al., 2015). Altogether,

these cores provide an ideal opportunity to characterize the influence of diagenesis on the Li isotope composition of platform carbonate sediments, typical of those preserved in the rock record. Moreover, all samples we study are younger than 8 Ma, and so formed during a period of time in which the δ^7Li value of seawater is not thought to have varied significantly from today (Hathorne and James, 2006; Misra and Froelich, 2012).

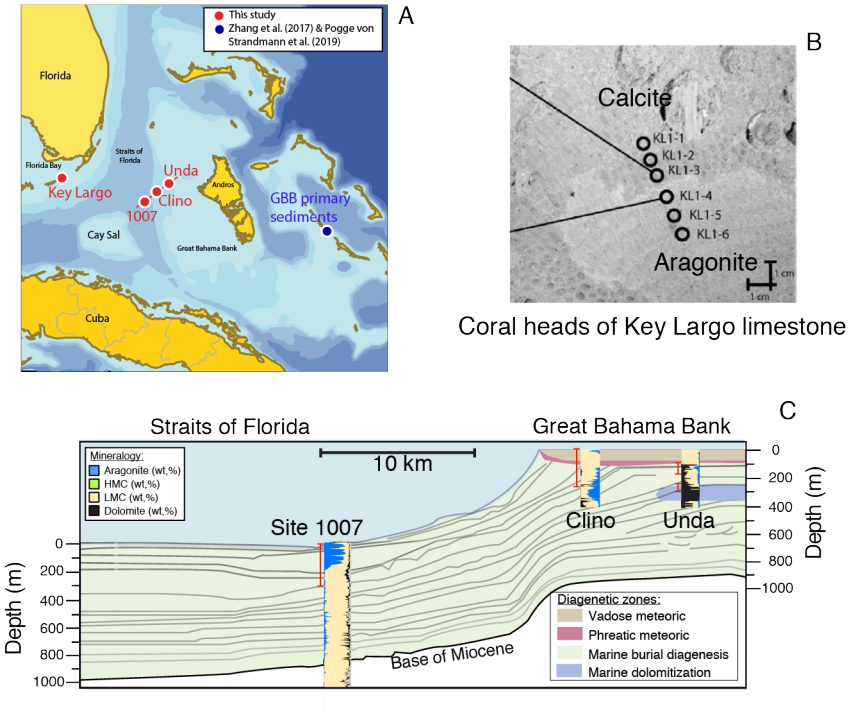

Figure 4. Location and characteristics of sample sites from this study. (A) Map with the location of Clino, Unda, Key Largo and 1007 core (modified from Swart, 2015). (B) Photograph of KL1 sample transect from the Key Largo Limestone and location of the samples. (C) Cross section of the GBB and location of Clino, Unda, 1007 and cores. The red vertical line indicates sample areas.

Table 1

Diagenetic conditions and main characteristics of the samples from this study

Diagenetic setting	References	Depositional Setting	Location	Age	Core depth	Mineralogy	Number of samples	Symbol in the figures
Bahamas platform								
Initial deposition	Zhang et al., (2017) & Pogge von Strandmann et al., (2019)	Bank top	Little Darby and Lee Stocking	Modern	-	Aragonite > HMC	23 & 26	○ & □
Meteoric	This study	Platform top	Clino	Pleistocene	23-150 m	LMC >> Aragonite	16	○
		Platform top	Unda	Pleistocene	90-107 m	LMC	6	○
Marine burial	This study	Platform top	Clino	Pleistocene	155-250 m	LMC > aragonite	7	□
		Platform top	Unda	Pleistocene	110-150 m	LMC > dolomite	17	□
		Platform top	Unda	Pliocene	274-292 m	Dolomite > LMC	12	□
		Toe of slope	1007 site	Pleistocene - Late Pliocene	23-150 m	Aragonite > LMC	14	△
		Toe of slope	1007 site	Early Pliocene - Late Miocene	200-350 m	LMC >> Aragonite	8	△
Key Largo								
Initial deposition	This study	Reef	Key Largo	Pleistocene	-	Aragonite	6	◇
Meteoric	This study	Reef	Key Largo	Pleistocene	-	LMC >> Aragonite	14	◇

3.1. Clino and Unda cores

The Clino and Unda cores—collected in 1990 during the Bahama Drilling Project (Ginsburg, 2001)—recovered periplatform carbonate sediments that are part of the margin of the Great Bahama Bank (Fig. 4) and cover a time period ranging from early Miocene (5.3 Ma) to the present-day. The original mineralogical composition of the carbonate is mainly aragonite (Reijmer et al., 2009), but the cores show well-defined meteoric diagenesis fronts, as well as deeper zones of dolomitization (Table 1; Melim et al., 2001; Swart and Melim, 2000). Repeated Pleistocene sea-level changes exposed the upper 120m of the carbonate platforms to the infiltration of

meteoric fluids and led to recrystallization of aragonite to meteoric LMC (Melim et al., 1995; Swart and Oehlert, 2018). Specifically, the uppermost 100 m in Clino and 60 m in Unda correspond to meteoric diagenesis in the vadose zone with dominantly meteoric LMC characterized by negative carbon and oxygen isotope excursions relative to the primary aragonite sediments in both cores (Melim et al., 1995; Swart and Oehlert, 2018; Stewart et al., 2015). The middle part (100-150 m for Clino, 60-107 m in unda) corresponds to the meteoric phreatic zone with increasing carbon and oxygen isotope composition with depth. The zone below 160 m in Clino and below 100 m in Unda is characterized by marine burial diagenesis with no subaerial exposure. In the marine burial diagenesis zone, both cores remain dominated by LMC but with minor dolomite mostly in Unda (in general < 5%, referred as "background dolomite, Swart and Melim, 2000) and up to 50% aragonite between 300 and 350m in Clino. Finally, between 250 and 350 m depth in Unda, there is a transition to a zone of pure dolomite of Pliocene age (referred as "massive dolomite").

3.2. Site 1007

Ocean Drilling Program (ODP) core 1007 was drilled in 1990 in the western margin of the Great Bahamas Bank as part of Leg 166 (Fig. 4). It is located in a more distal part of the bank than Clino and Unda cores, on the toe-of-slope of the western GBB, under 647 m of water (Eberli and Swart, 1997). The core has a total depth of 1250 m, covering the entire Neogene and the early Oligocene. Contrary to Clino and Unda, the 1007 core has not been exposed to meteoric diagenesis. In the upper 150-200m, the mineralogy is dominated by aragonite (about 70-80%), but below this depth, the proportion of aragonite drops to less than 20% with most of the mineralogy being low-Mg calcite, with minor proportions of dolomite (Fig. 4). We note that contrary to the Clino and Unda cores, there is a minor proportion of non-carbonate phases, mostly between 0 and 10% (median of 5%) with a few samples having more than 20% non-carbonate phases. The transition from aragonite- to LMC-dominated sediments is accompanied by a decrease of the carbon isotope composition from 4-5‰ at the top of the core to a minimum of 1-2‰ at 350m (Swart and Eberli, 2005), and this change has been interpreted as reflecting a change in the source of the sediments from dominantly LMC pelagic carbonates before the late Pliocene to aragonitic peri-platform sediments in the late Pliocene and Pleistocene (Swart, 2008; Swart and Eberli, 2005). Recent work investigating Ca and Mg isotopes on the same core (Higgins et al., 2018) temper these conclusions by highlighting that some of these mineralogical and geochemical changes are also the result of change in the diagenesis style, from sediment to fluid-buffered diagenesis. Here, we analyzed 22 samples between 23 and 350 m depth, all younger than 8 Myr.

3.3. Key Largo Limestone

The Key Largo Limestone occurs in the southern part of Florida and formed from patch reefs that started growth about 120,000 years ago, during the last interglacial (Multer et al. 2002). This unit has been continuously exposed to meteoric fluids since the onset of the Wisconsinan regression, ~100,000 years ago and shows varying degrees of aragonite-to-calcite alteration and variable calcite cementation (Gill et al., 2008; Multer et al. 2002). The samples on which we measured the δ^7Li are the same as those used by Gill et al. (2008). The carbonate powder was collected by drilling the original aragonite and the secondary calcite on the coral heads of the species *Orbicella annularis* (formerly *Montastrea annularis)* (Gill et al., 2008). Previous characterization of these samples has shown that the geochemical alteration signature in Key Largo samples has evolved over time, likely in response to the evolution of the overlying vadose zone (Gill et al., 2008).

4. Analytical methods

For Clino, Unda and the Key Largo limestone we worked with the same carbonate powder samples as used in prior geochemical studies (Hardisty et al., 2017; Liu et al., 2019; Chen et al., 2018; Gill et al., 2008). About 10-20 mg of sample was pre-leached, following the same method as in Dellinger et al. (2018), to remove exchangeable ions using 1N ammonium acetate followed by 3 rinses with 18.2 megaOhm (millipore) water. The samples were then digested in dilute hydrochloric acid (HCl 0.05N) for 30 minutes to an hour. The volume of acid used for digestion was calculated to dissolve 30 to 95% of the sample (depending upon the silicate proportion) in order to minimize the leaching of non-carbonate phases. After the digestion, the supernatant was collected while the sample residue was weighed in order to determine the yield of the digestion. Ratios of trace elements relative to Ca were

measured using a Thermo Scientic Element 2 inductively coupled plasma mass spectrometer (ICP-MS) at the Yale Metal Geochemistry Center following a method adapted from Misra et al. (2014). All samples and standards were measured at a Ca concentration of 50 ppm. The instrument was first conditioned for 1 hour with a solution of 50 ppm Ca. A set of 5 to 10 multi-elemental calibration standards was measured at the beginning of the run, and a bracketing standard solution was measured every 5 to 10 samples to correct for the drift of the signal. Accuracy and precision of analyses were checked using the aragonite reference material FEBS-1 (NRC) and in-house prepared standard solutions matching typical calcium carbonate chemical composition. Analytical precision was between 5 and 15%, depending on the element and the concentration.

For the Li isotope analyses, Li was separated from the rest of the sample matrix chromatographically at the Yale Metal Geochemistry Center using 2.7 mL of AG50W-X12 resin following the method used in Dellinger et al. (2014). A mass of 1 to 40 ng of Li was introduced into the column (in 0.5 mL 0.2N HCl) and Li was eluted with 40 mL of 0.2N HCl. The total procedural blank for Li isotope analysis was ~ 0.02 ng Li (n=5 blanks), which is insignificant compared to sample Li. Sodium concentration in the elution fraction was checked before every isotope analysis, and samples having Na/Li ratio higher than 5 were processed through a second column. Lithium isotope ratios were measured using a Thermo Scientic Neptune Plus multiple collector inductively coupled plasma mass spectrometer (MC-ICP-MS) using an APEX desolvation system at the Yale Metal Geochemistry Center. Most samples were successively measured 2 consecutive times within a standard-sample bracketing (SSB) sequence with ratios reported in delta notation relative to LSVEC. For each sample and bracketing standard, $^{7}Li/^{6}Li$ ratios were measured for 50 cycles of 4 seconds each. With this setup, the sensitivity was 0.6V/ppb Li and measured samples had signal intensity ranging from 0.4 to 8.0 V (average of 3.5V), depending of the amount of Li in the sample. Background intensities (usually stable during a whole sequence of several hours) were measured before and after each bracketing standard, sample intensities were corrected for the background signal. The blank intensity of the background was no more than 0.2–1% of the sample intensity. The internal standard error of sample measurements (average of ±0.08‰, 2σ) was typically between ±0.05‰ for high Li beam intensity to ±0.40‰ (2σ) for low beam intensity. Atlantic Seawater (OSIL) was measured as a reference standard to check the accuracy of the data and returned an average $\delta^{7}Li$ value of 31.2±0.6‰ (2σ, n=7 different aliquots processed through column chemistry), in good agreement with average data from the literature. We also measured the $\delta^{7}Li$ of the NRC carbonate standard FEBS-1 and obtained a $\delta^{7}Li$ value of 15.8±0.4‰ (n=2). Overall, we consider a maximum uncertainty of ±0.8‰ (2σ) on $\delta^{7}Li$ for all samples.

5. Results

5.1. Meteoric diagenesis zone

Results for Li isotopes and Li, Ca, Mg, Sr, Mn, Al, and Fe contents are presented in table (2). The samples from the meteoric diagenesis zone of Clino and Unda have a range of $\delta^{7}Li$ values that span 13‰, with values from +16.2 to +29‰ in Clino and from +21 to +29‰ for Unda (Fig. 5). The bulk meteoric vadose zone $\delta^{7}Li$ value is +22.1±3.0‰ (1σ, n=13), indistinguishable from the inferred original $\delta^{7}Li$ value of the GBB sediments ($\delta^{7}Li$ = +22±1‰; Fig. 5) but showing a much wider range. The average $\delta^{7}Li$ value in the phreatic zone (+24.4±3.7‰; 1σ, n=9) is slightly higher than in the vadose zone and increases with depth from a value of +17‰ to values of about +27‰ at higher depth. The average Li/(Ca+Mg) ratio of the vadose zone samples is 4.9±1.1 $\mu mol.mol^{-1}$ (1σ, n=13), and 3.3±1.3 $\mu mol.mol^{-1}$ (1σ, n=10) for the phreatic zone samples, both lower than the Li/(Ca+Mg) ratio of the unaltered platform carbonates (9±1 $\mu mol.mol^{-1}$). In Clino and Unda, the Li/(Ca+Mg) ratios decrease from about 4-5 $\mu mol.mol^{-1}$ at the top of the phreatic zone to values of 1 $\mu mol.mol^{-1}$ at the bottom, before increasing again at the transition to marine burial diagenesis. Measured Al/(Ca+Mg) ratios are generally low (0.01 to 0.25 $mmol.mol^{-1}$) and on average only slightly higher than in the GBB sediments (Fig. 5).

In the Key Largo Limestone, the bulk average $\delta^{7}Li$ value of the meteoric-altered samples is 18.1±2.2‰ (1σ, n=6) which is indistinguishable from the non-altered value 17.9±0.7‰ (1σ, n=5), but the range and standard deviation are larger (Fig. 6). The Li/(Ca+Mg) ratios of the unaltered aragonite samples ranges from 4.9 to 6.5 $\mu mol.mol^{-1}$, averaging 5.7±0.6 $\mu mol.mol^{-1}$ (1σ, n=7). These values are similar to the Li/Ca ratios observed in corals (Rollion-Bard et al., 2009). The Li/(Ca+Mg) ratios of altered low-Mg calcite samples is much lower, 0.3 to 3.7

µmol.mol^{-1} except for sample KL12-6 which has similar Li/(Ca+Mg) ratios as unaltered aragonite. The average Li/(Ca+Mg) ratios of the altered material is 1.6±1.4 µmol.mol^{-1} (1σ, n=15).

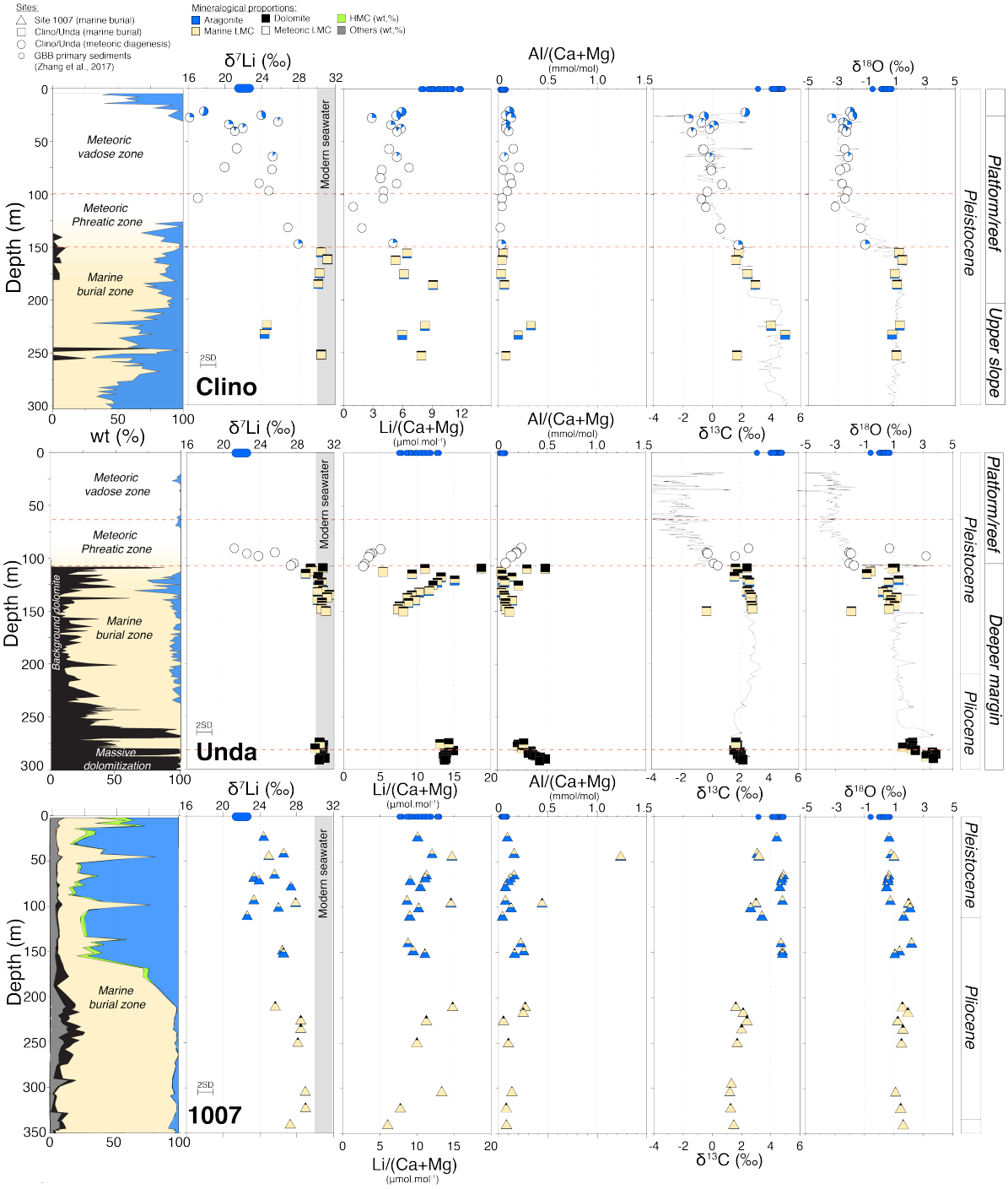

Figure 5. Carbonate mineralogy, δ^7Li, and Li/(Ca+Mg), Al/(Ca+Mg), δ^{13}C and δ^{18}O versus depth for the Clino (top), Unda (middle) and 1007 cores (bottom). The mineralogy and lines for δ^{13}C and δ^{18}O come from Melim et al. (1995). Carbon and oxygen isotope data for our specific samples are superimposed (data from Hardisty et al., 2017). The filling of the points corresponds to the mineralogical proportions. The vertical grey bar corresponds to the modern seawater δ^7Li value.

5.2. Marine diagenesis zone

In both the Clino and Unda cores, δ^7Li values increase with depth at the transition between the meteoric and the marine burial diagenetic zone (Fig. 5). The δ^7Li values in the marine diagenesis zone of the Clino and Unda cores is ~30-31‰ (+30.2±1.5‰, 1σ, n=36), identical within uncertainty to the δ^7Li values of modern seawater.

Two Clino samples characterized by high proportions of aragonite have low δ^7Li of +24.5‰. Below 280 m in the Unda core, there is a zone entirely composed by dolomite (massive dolomite) with an average δ^7Li value of +30.6±0.3‰ (1σ, n=12), also identical to modern seawater. The δ^7Li values in ODP Site 1007 samples range between +22.0 to +29.6‰, with a progressive increase in δ^7Li value with depth. We observe a positive relationship between the δ^7Li and the wt% proportion of LMC in 1007 samples (Fig. 7B). The Li/(Ca+Mg) in the marine diagenesis zone is generally higher in Unda (from 5 to 19 µmol.mol^{-1}) and in 1007 site (6 to 20 µmol.mol^{-1}) relative to Clino (5 to 9 µmol.mol^{-1}). In Unda, we observe a peak of high Li/(Ca+Mg) ratios that coincides with the peak of dolomite proportion (hardground dolomite sample) at the transition between the meteoric and marine diagenesis zones. For Clino and Unda Pleistocene sediments, the Li/(Ca+Mg) ratio of samples from the marine diagenesis zone in both cores is positively correlated with the proportion of dolomite and inversely correlated with the proportion of low-Mg calcite (r^2=0.81 excluding 1 sample, Fig. 7A). In contrast, no clear relationship between Li/(Ca+Mg) and the proportion of LMC is observed for samples from site 1007 (Fig. 7A). For Clino and Unda, measured Al/(Ca+Mg) ratios are generally low (0.01 to 0.50 mmol.mol^{-1}) with high values only observed in dolomite rich samples (Fig. 5 and Appendix A3). As discussed in the Appendix (A3), samples having Al/(Ca+Mg) ratios > 0.45 mmol.mol^{-1} are potentially influenced by silicate contamination during digestion of the sediments and are therefore excluded from the rest of the discussion. This cutoff value is half that used in other studies (e.g. Al/Ca of 0.80 mmol.mol^{-1} in Pogge von Standmann et al., 2013; Bastian et al., 2018).

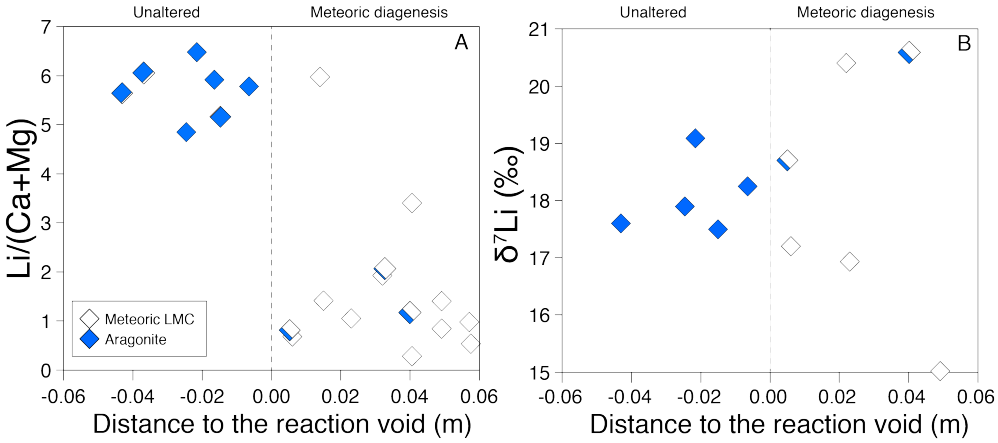

Fig. 6. Meteoric diagenesis alteration profile for (A) Li/(Ca+Mg) (in µmol.mol^{-1}) and δ^7Li (B) in Key Largo limestone. The alteration front in these samples (distance = 0 m on the x-axis) represents a shift from aragonite to low-Mg calcite. The filling of the points corresponds to the mineralogical proportions.

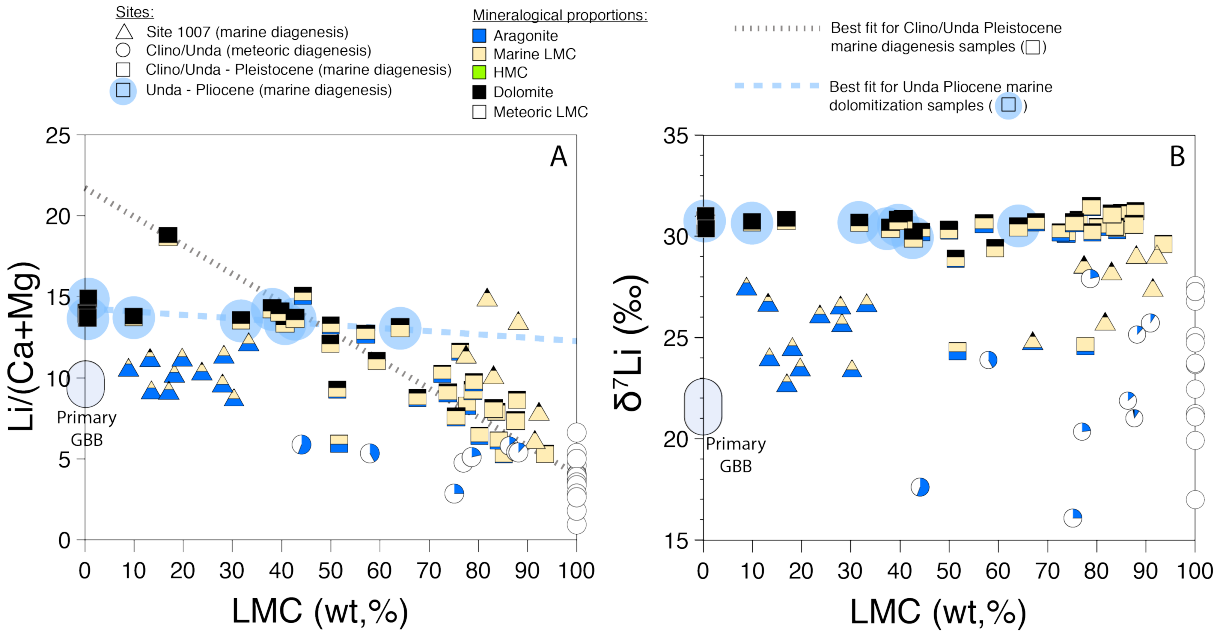

Fig 7. Mineralogical control on Li isotope composition and Li/(Ca+Mg) value (in µmol.mol^{-1}) for the samples from this study. (A) Proportion of Low-Mg calcite (LMC) as a function of the Li/(Ca+Mg) ratio and (B) δ^7Li. The blue dotted line corresponds to the best fit for Pliocene Unda samples from the massive dolomite zone (squares with blue circle), whereas the grey dotted line corresponds to the best fit or Clino and Unda samples from the marine burial zone (squares with no blue circle, r^2=0.81 excluding the Clino sample at 232.96m having high proportion of aragonite). The filling of the points corresponds to mineralogical proportions.

6. Discussion

6.1. Influence of marine burial diagenesis on δ^7Li

In this section, we focus first on observations from the marine burial diagenesis zone. The average δ^7Li value of the marine burial samples (+30±1.5‰) from Clino and Unda is identical within uncertainty to the δ^7Li value of modern seawater, but about 8‰ higher than the original δ^7Li value of GBB aragonitic sediments (Fig. 5). Thus, marine burial diagenesis imparts a modern seawater-like composition on the Clino and Unda carbonates. However, the same is not true for the periplatform carbonates from the 1007 core, where δ^7Li values vary from +23.3 to +28.6‰. In addition to different δ^7Li values, Clino/Unda and 1007 sediments define very distinct geochemical trends between δ^7Li values and other geochemical proxies, particularly Li/(Ca+Mg) and Sr/(Ca+Mg) ratios, as well as δ^{13}C and δ^{18}O (Fig. 8). The observed variability of δ^7Li values and Li/(Ca+Mg) ratios with respect to depth and the differences between Clino/Unda and Site 1007 result from the combination of two processes: i) diagenetic resetting of primary aragonite signatures during conversion of LMC and dolomite under fluid-buffered vs. sediment buffered conditions and/or ii) changes in the source of the carbonate sediment (pelagic calcite vs. platform aragonite carbonates) with time and distance to the GBB platform (i.e., with more pelagic contribution at in the periplatform setting of 1007). Below we discuss the respective influence of these two processes. Overall, we attribute the Clino and Unda Li isotope signatures to diagenetic resetting, and the distinct 1007 patterns to a combination, with at least some influence from variable amounts of primary pelagic calcite.

In detail, the bulk Li/(Ca+Mg) of Clino/Unda Pleistocene sediments is controlled by a mineralogical mixture between Li-poor LMC and Li-rich dolomite (fig. 7A). The correlation between Li/(Ca+Mg) and wt% LMC (r^2=0.81, fig. 7A) suggests the LMC component in these samples (intercept at 100% LMC of the mineralogical mixing trend of Figure 7A) has a relatively homogeneous composition with a Li/(Ca+Mg) value of 4±2 µmol.mol^{-1}, a δ^{13}C value of ~2.2‰, and a Sr/(Ca+Mg) ratio ~2.0 mmol.mol^{-1} (Fig. 8). All these values, particularly the low Li/(Ca+Mg) and the high δ^7Li, are compatible with fluid-buffered diagenesis (with respect to Li, but also Sr, C, and O; see section 2). Inorganic LMC precipitated from seawater should have lower Li/Ca than aragonite due to lower Kd^{Li} (section 2), as observed in these samples. Interestingly, these samples have Li isotope ratios ~30-31‰. Fluid-buffered diagenetic calcite derived from pore waters with a seawater-like δ^7Li value (~+31‰) should form

with δ^7Li = 27-30‰ ($\Delta^7Li_{LMC\text{-}fluid}$ ~ −1-4‰; Marriot et al., 2004b; Pogge von Strandmann et al., 2017). Thus, our observation of diagenetic carbonates at ~30-31‰ requires either a fractionation factor at the very lower end of those experimentally determined for LMC, or pore waters that are ~2‰ heavier than seawater (due to influence of other processes). In any case, the diagenetic LMC from the burial diagenesis sections of these cores carries a uniform δ^7Li, similar to ambient seawater composition.

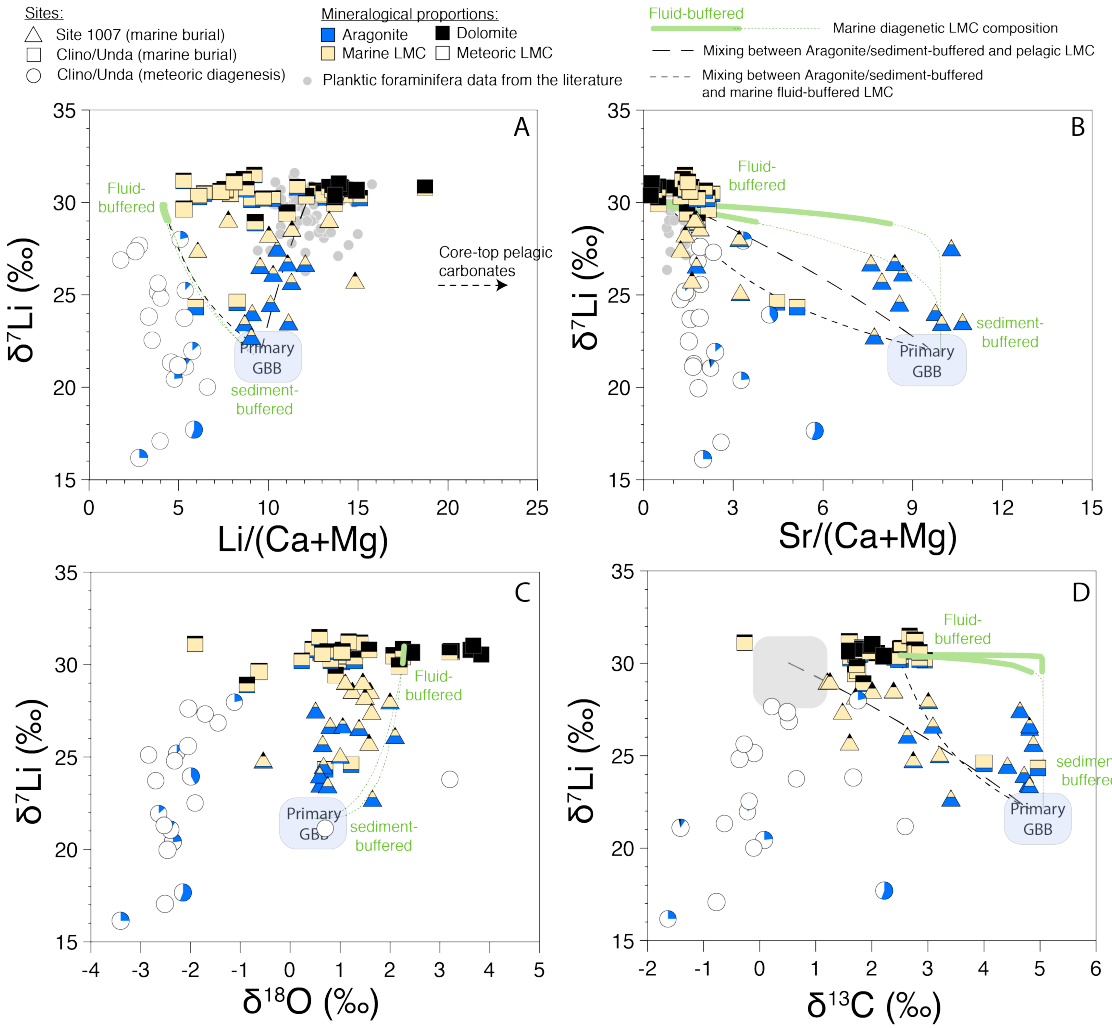

Fig. 8. Diagenetic covariation cross-plots between Li isotope composition and (A) the Li/(Ca+Mg) ratio (in µmol.mol^{-1}), (B) the Sr/(Ca+Mg) ratio (in mmol.mol^{-1}), (C) $\delta^{18}O$ and (D) $\delta^{13}C$ of carbonates. Samples from the Key Largo Limestone are not shown. The thick green lines correspond to the fluid-buffered diagenetic end-member (in regard to Li, $dEQ^{Li} > 0.9$). The thin green lines in each panel correspond to the whole compositional range of diagenetic end-member values calculated both for no advection rate and high advection rate (see Appendix A1). The black dotted lines are mixing lines between primary GBB and the inferred composition for pelagic carbonates and fluid-buffered marine LMC (in regard to all proxies, i.e. dEQ^C, EQ^O, EQSr > 0.9). Li isotope data for planktic foraminifera are from Hall and Chan (2005), Hathorne and James (2006) and Misra and Froelich (2012). The $\delta^{13}C$ and $\delta^{18}O$ values for Site 1007 and inferred range of $\delta^{13}C$ for planktic foraminifera are from Swart and Eberli (2005).

The higher Li/(Ca+Mg) ratio for dolomite-rich Clino/Unda samples (up to 15-22 µmol.mol^{-1}) suggests that dolomite that precipitated under fluid-buffered conditions in the cores (Ahm et al., 2018) incorporated a higher proportion of Li than diagenetic LMC. In detail, we note that the intercept at 0 wt% LMC (or 100 wt% dolomite; Fig. 7) is distinct for Pleistocene sediments relative to Pliocene sediments. In other words, the Li/(Ca+Mg) of Pliocene massive dolomites (15±2 µmol.mol^{-1}) is lower than the Li/(Ca+Mg) of the background dolomite in the younger samples (~22 µmol.mol^{-1}). These differences are consistent with a distinct origin of the two different type of dolomites inferred from their different Sr/Ca ratios and $\delta^{18}O$ values (Swart and Melim, 2000). However, both dolomites have a seawater-like δ^7Li value similar to that of the fluid-buffered LMC, instead of low δ^7Li as would

be predicted (section 2) from the recently reported fractionation factor between inorganic dolomite and the fluid of –23±6‰ at 25°C (Taylor et al., 2019). Precipitation of dolomite with a δ^7Li value of +31‰ as we observe would, given this fractionation factor, require a fluid with δ^7Li of +54‰; such enriched δ^7Li has only been measured in a few marine pore fluid samples (Scholz et al., 2010). Independent arguments suggest that the fluid that precipitated the Unda massive dolomite was seawater with "normal composition" (Swart and Melim, 2000: Ahm et al., 2018). In addition, the consistently narrow range of δ^7Li values we observe in dolomites, around +31‰, match present-day seawater, even though we have sampled a range of dolomites from different depths, cores, and likely mechanisms of precipitation (Swart and Melim, 2000). Altogether, our results point toward a more modest dolomite-fluid Li isotope fractionation factor than extrapolated from high-temperature experiments. At this stage, we cannot completely exclude a dolomite precipitating from a seawater derived fluid with very high δ^7Li values and with a very large fractionation factor (Taylor et al., 2018), and more experimental and empirical studies on dolomite will be necessary to ultimately resolve this question.

Finally, we observe that some LMC-rich samples (that contain low amounts of dolomite and aragonite), particularly from Site 1007, have Li/(Ca+Mg) ratios higher and δ^7Li lower than the inferred fluid-buffered diagenetic end-member (Fig. 8). One possibility to explain this signature is that these samples contain pelagic LMC, since modern foraminifera have δ^7Li ~30‰ and Li/(Ca+Mg) ~10-16 µmol.mol^{-1} (see Fig. 8A) and bulk top core pelagic carbonates from the Bahamas have δ^7Li ~24-27‰ and Li/(Ca+Mg) ~20-40 µmol.mol^{-1} (Pogge von Strandmann et al., 2019). A substantial contribution of pelagic material to the 1007 samples is consistent with the conclusions of Swart and Eberli (2005) based on the carbon isotope composition. This interpretation also fits observed mixing trends (Fig. 8). An alternative possibility is that the high Li/(Ca+Mg), low δ^7Li carbonates contain LMC formed during more sediment-buffered diagenesis conditions than Clino and Unda, as has been suggested to explain their Ca isotope composition (Higgins et al., 2018). Transformation of aragonite to LMC under sediment-buffered diagenetic conditions should produce LMC with similar geochemical composition as the original aragonite (δ^7Li ~23‰ and Li/(Ca+Mg) ~8-12 µmol.mol^{-1}). In fact, diagenetic minerals can have compositions that range from pure fluid-buffered to pure sediment-buffered signatures (section 2 and Fig. 8). Some LMC-rich samples plot within both the diagenetic trend (green curves) and on the mixing trend (black dotted curve) between fluid- and sediment-buffered marine LMC (Fig. 8). However, the presence of aragonite in Plio-Pleistocene Site 1007 samples between 0 and 170 mbsf makes it difficult to quantify more precisely the contribution of primary vs. diagenetically-formed LMC in the top 200m of core 1007, since the aragonite has not yet been completely transformed into low-Mg calcite or dolomite by early diagenetic processes at this site.

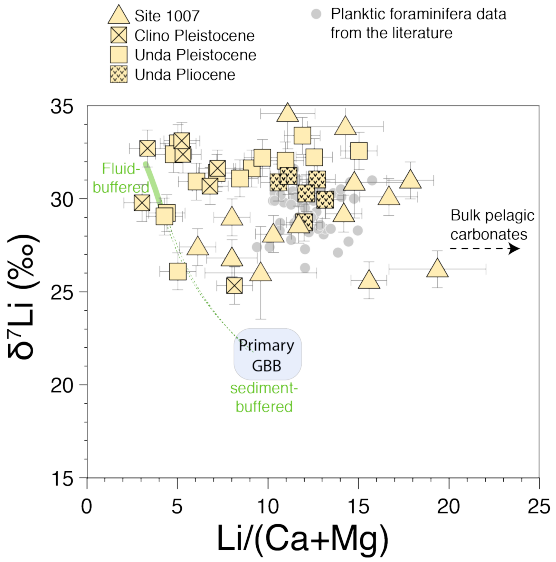

Fig. 9. Calculated geochemical composition (δ^7Li and Li/(Ca+Mg) in µmol.mol^{-1}) of the LMC component for each sample (see supplementary data table). The diagenetic end-members are the same as in Fig. (8A).

Given that we seek to determine the extent to which diagenesis overprints or preserves the primary seawater signal, we use a simple isotope mass-balance attempt to calculate the composition of the LMC component only. We do so by correcting for aragonite and dolomite contribution to all samples from the marine diagenetic

zone at Site 1007 and Clino-Unda (see appendix A3 for details and supplementary table for results). In this manner, we can determine whether the diagenetic LMC records the signature of seawater or not. Results are shown in Figure 9, along with the range of expected values for fluid-buffered and sediment buffered diagenetic LMC formed in marine pore fluids. The δ^7Li-Li/(Ca+Mg) variability is well-explained by a 3-component mixture between i) fluid-buffered diagenetic LMC (Li/(Ca+Mg) ~ 3-5 μmol.mol^{-1}, δ^7Li ~ 29-32‰), ii) sediment-buffered diagenetic LMC (same composition as GBB platform top sediment, Li/(Ca+Mg) ~ 9 μmol.mol^{-1}, δ^7Li~23‰) and iii) pelagic LMC (Li/(Ca+Mg) ~ 13-20 μmol.mol^{-1}, δ^7Li~31‰). Note that some samples have δ^7Li values higher than +31‰ which might be due to the large uncertainty associated with these isotope mass-balance calculations. For Clino, we observe that all Pleistocene sediments (except one) plot close to the fluid-buffered end-member. For Unda, the Pleistocene samples are between the fluid-buffered and pelagic end-members while the Pliocene sediments plot closer to the pelagic end-member. Finally, for Site 1007, samples are mostly between the diagenetic component with values intermediate between fluid- and sediment- buffered compositions and a pelagic end-member.

In summary, the observed diagenetic transformation of δ^7Li values implies that the Unda and Clino cores were subject to more open-system alteration during marine burial diagenesis than the 1007 samples, supporting interpretations from previous studies (Henderson et al., 1999; Higgins et al., 2018). This difference is probably the result of higher fluid advection rate close to the GBB (Caspard et al., 2004; Higgins et al., 2018). Altogether, the δ^7Li values of the non-meteoric Bahamian carbonates reflect largely what we would expect: where fluid-rock ratios are high, open-system diagenesis imparts a consistent seawater-like δ^7Li values on the buried carbonate (Clino and Unda), but where closed-system diagenesis is rock-buffered, δ^7Li can be variable, reflecting the different mineralogy-dependent fractionation factors.

6.2. Meteoric diagenesis

6.2.1. Evidence for diagenetic resetting of carbonate δ^7Li in the meteoric zone

The average Li isotope ratio from carbonates in the meteoric alteration zone of Clino and Unda (δ^7Li = +22.0±3.8‰; 1σ, n=28) is similar to primary aragonite-dominated carbonate sediment from this region. The same is true for the Key Largo samples. It is thus tempting to interpret these samples as recording primary Li isotope signatures of aragonite (as might be the case for sediment-buffered diagenesis). However, other geochemical proxies (δ^{13}C, Sr/Ca, Mg/Ca) that are less sensitive to meteoric diagenesis than Li (according to calculations from section 2) have fluid-buffered composition and show resetting in these samples (Gill et al., 2008; Melim et al., 2001; Stewart et al., 2015). Moreover, the δ^7Li and Li/(Ca+Mg) from samples in the meteoric zone are negatively correlated with the δ^{13}C (Fig. 8D and 10A). Thus, we expect Li to also be reset to the meteoric fluid composition. In addition, the Li/(Ca+Mg) ratio is lower in carbonates from the altered zone than in primary Bahamas carbonates (Fig. 8), which is expected from diagenetic transformation of aragonite to calcite (see section 2). Together, these trends indicate LMC precipitation in the presence of meteoric fluids, consistent with conclusions from data on other isotopic systems such as C, O, Sr, U and B that implies high fluid-rock ratios (Melim et al., 1995; Stewart et al., 2015; Swart and Oehlert, 2018; Chen et al., 2018). Therefore, we conclude that meteoric diagenesis in Clino, Unda and Key Largo has altered the primary Li signature, producing variable isotopic compositions controlled by meteoric fluid composition. The resulting carbonates have δ^7Li values that are 3 to 15‰ lower than corresponding seawater and marine fluid-buffered diagenetic LMC, but coincidently similar on average to primary GBB aragonite.

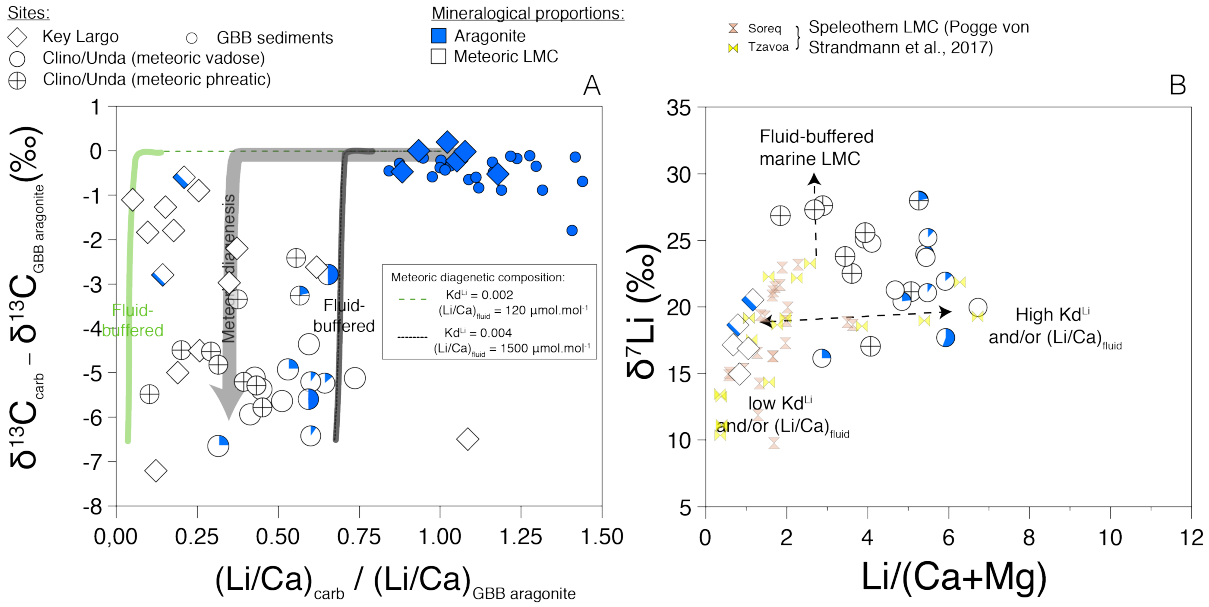

Figure 10. Effect of meteoric diagenesis on Li/Ca and Li isotopes. A) Carbon isotopes of Clino, Unda and Key Largo meteoric diagenesis zone corrected from the carbon isotope value of the original aragonite ($\delta^{13}C_{carb} - \delta^{13}C_{aragonite}$) as a function of the (Li/Ca) ratio of the samples divided by the original (Li/Ca) of the aragonite carbonate. Values of $(Li/Ca)_{carb}/(Li/Ca)_{GBB\ aragonite} < 1$ indicates loss of Li during diagenesis. B) δ^7Li as a function of the Li/(Ca+Mg) (in µmol.mol^{-1}) for meteoric diagenesis samples only. Soreq and Tzavoa travertine samples from Pogge von Strandmann et al., (2017) are also represented.

6.2.2. Control of the δ^7Li and Li/Ca in the meteoric zone

If we accept that the Li system has been reset in the meteoric portions of the Clino and Unda cores, and in the Key Largo Limestone, then based on mass balance predictions (see Section 2), the δ^7Li values and Li/Ca ratios of carbonate in these zones should depend on a combination of (1) the composition of the meteoric fluid itself, which is controlled by soil processes including Li supply from carbonate and minor silicate components (detrital or dust), along with fractionation during Li retention in secondary phases (clay minerals, iron oxides); and (2) the partition coefficient and fractionation factor during formation of the diagenetic carbonates, which may vary to some extent as a function of salinity, temperature, and pH (see section 2). The causes of the 12‰ variability within the meteoric diagenetic zone, in particular the differences between the Clino vadose zone (low δ^7Li values and high Li/Ca ratios), the Clino-Unda phreatic zone (high δ^7Li values and low Li/Ca ratios) and the Key Largo limestone (low δ^7Li values and low Li/Ca ratios), are not known but could be related either to local processes (e.g. style of weathering in the overlying soils) or global factors (e.g. climatic changes) (Fig. 10).

A comparison with speleothem data from Soreq and Tzavoa caves in Israel (Pogge von Strandmann et al., 2017) may hold some clues. In the δ^7Li –Li/Ca space (Fig. 10), the Key Largo samples plot in the middle of the trend defined by the majority of Soreq and Tzavoa samples, indicating that their composition can be explained in the same way, i.e., by variability in the congruency of meteoric weathering (Pogge von Strandmann et al., 2017) – meaning that climatic variability and other factors that control weathering congruency can impart highly variable δ^7Li (by 10‰ or more) on carbonates that have been exposed to meteoric diagenesis. However, some of the Soreq and Tzavoa samples (n=7), along with the Clino samples from the vadose zone, have much higher Li/Ca ratios (3 to 7 µmol.mol^{-1}). Such high Li/Ca ratios in carbonates would require calcite precipitation from fluid having much higher Li/Ca ratios (1500 to 5000 µmol.mol^{-1}) than typical Li/Ca ratios of rivers draining limestones and/or a much higher Kd^{Li}. We expect that such high Li/Ca is therefore more likely the result of changes in local environment conditions, e.g. local evaporation of meteoric fluids under drier climatic conditions, increased contribution of silicate phases, mixing with a small proportion of seawater fluids, or effects from local variability in pH and temperature influencing Kd^{Li}. Hence, the Clino samples from the vadose zone may have been affected by specific local porewater environments. Finally, we observe that sample from the meteoric phreatic zone in Clino and Unda have in general the highest δ^7Li among meteoric LMC samples. A possible explanation is that phreatic meteoric LMC records the progressive change of the δ^7Li and Li/Ca between LMC formed under meteoric alteration conditions and LMC formed under marine fluid-buffered conditions (Fig. 10B). This hypothesis would be in

agreement with the proposed explanation for the co-variation of $\delta^{13}C$ and $\delta^{18}O$ in this zone (Swart and Oehlert, 2018). Regardless of the specific mechanism explaining differences between the vadose and phreatic zones, it is clear that meteoric diagenesis is imparting highly variable $\delta^{7}Li$ and Li/Ca in altered carbonates and is likely to pose challenges in reconstructing past seawater composition from meteorically altered carbonates, although well-targeted studies may be able to harness this variability to infer information about local weathering and climatic conditions.

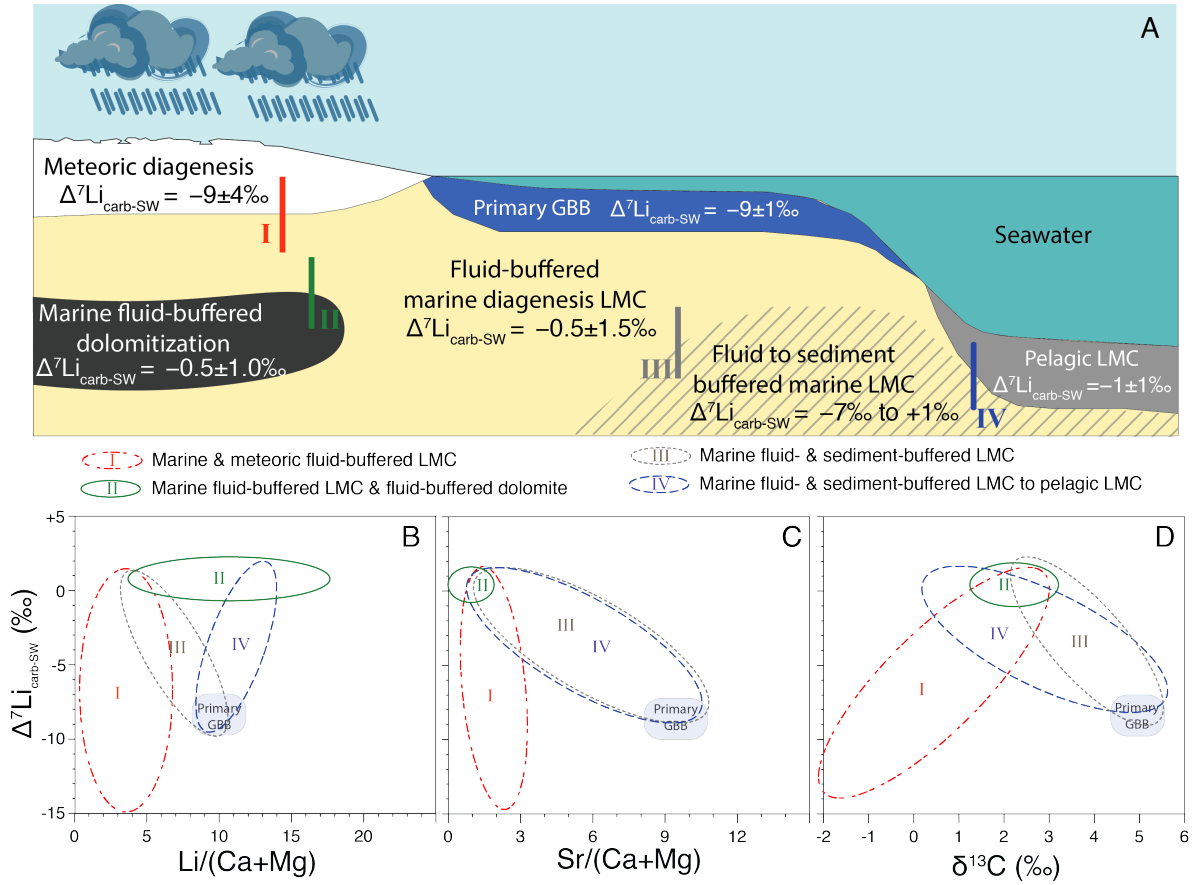

Figure 11. Summary of the influence of diagenesis on Li isotopes in the Bahamian platform. A) Range of Li isotope composition ($\Delta^{7}Li_{carb\text{-}sw} = \delta^{7}Li_{carb} - \delta^{7}Li_{sw}$) of primary, pelagic and diagenetic carbonates in the Bahamas. Note that the geographical locations of diagenetic zones is schematic and not representative of the actual location of different types of carbonates in the Bahamas platform. The panels B, C and D are cross-plots between $\Delta^{7}Li_{carb\text{-}sw}$ and Li/(Ca+Mg), Sr/(Ca+Mg) and $\delta^{13}C$. Are also represented schematic examples of transition and/or mixture of (I) marine and meteoric fluid-buffered LMC (e.g. Clino core), (II) marine fluid-buffered LMC and dolomite (e.g. Unda core 100-150 m), (III) marine fluid-buffered LMC and sediment-buffered LMC and (IV) marine fluid- to sediment-buffered LMC and pelagic LMC (e.g. Site 1007).

7. Implications and guidelines for interpreting the $\delta^{7}Li$ values of ancient carbonates

Our new data and analysis show that diagenetic transformation of aragonite to LMC produces a wide range of Li isotopic composition and Li/(Ca+Mg) ratios in altered carbonate from the Bahamas. These observations have important implications for reconstructing the past $\delta^{7}Li$ of the ocean using marine carbonates. In Fig (11), we summarize the observations about the effects of diagenesis in the Bahamas from this study, and in Table 3 we provide general quantitative predictions (i.e. for any ancient carbonate) for how each type of diagenetic processes may affect $\delta^{7}Li$ and other geochemical proxies. We suggest that this framework can serve as a road map for identifying ancient samples recording reliable seawater $\delta^{7}Li$. We express the $\delta^{7}Li$ in terms of difference between carbonates and corresponding seawater ($\Delta^{7}Li_{carb\text{-}sw} = \delta^{7}Li_{carb} - \delta^{7}Li_{sw}$) with a $\Delta^{7}Li_{carb\text{-}sw}$ value of 0‰ indicating that the $\delta^{7}Li$ of carbonates is the same as corresponding $\delta^{7}Li$ of seawater. In the Bahamas, we have identified four types of diagenetic mineral formation pathways:

i) Marine LMC and dolomite formed in fluid-buffered conditions ($dEQ^{Li} > 0.9$) have the composition of marine porewaters and yield remarkably consistent δ^7Li that reliably record seawater composition at the time of diagenetic alteration, even following dolomitization ($\Delta^7Li_{carb\text{-}sw} \sim -0.5\pm1.5‰$). Importantly, these do not record seawater composition at the depositional time of the unit, since the seawater-like signature is acquired during diagenetic transformation rather than primary crystallization. If carbonates have $\delta^{44}Ca$, $\delta^{13}C$ and Sr/(Ca+Mg) values that are not completely sediment-buffered ($\delta^{13}C \sim +2‰$, $\delta^{44}Ca > -1.5‰$, Sr/Ca < 2 mmol.mol^{-1}; Ahm et al., 2018) this can be seen as strong evidence for fluid-buffered diagenetic conditions for Li isotopes, and at least based on the results from the Bahamas, we expect such samples to reliably and directly record seawater δ^7Li composition (Table 3). In addition, LMC from marine fluid-buffered diagenesis has low Li/(Ca+Mg) (2-6 μmol.mol^{-1}) relative to most marine carbonates (Dellinger et al., 2018) while dolomite has higher Li/(Ca+Mg) (15-20 μmol.mol^{-1}).

We note that for periods of time when the rate of change in seawater δ^7Li value was slow (i.e. the Cenozoic record) relative to the timescale of sediment diagenesis after initial carbonate formation (i.e. time between carbonate precipitation and diagenesis), marine fluid-buffered diagenesis is likely to preserve the composition of seawater. However, for short events where the marine δ^7Li values likely varied (e.g. the Ocean Anoxic Events of the Mesozoic), fluid-buffered diagenetic carbonates may recrystallize from a marine porefluid having distinct δ^7Li value relative to the marine δ^7Li value at the time of the deposition of the original carbonate (before diagenesis), and hence may not preserve the original marine δ^7Li value.

ii) Marine LMC formed in a continuum and/or by a mixture of fluid- to sediment-buffered conditions ($0.1<dEQ^{Li}<0.9$) records δ^7Li that is not necessarily reset to a seawater value. Thus, these carbonates have a variable and lower isotopic composition relative to seawater ($\Delta^7Li_{carb\text{-}sw} \sim -15$ to $-3‰$). Carbonates formed in these diagenetic conditions would usually have Sr/Ca > 2 mmol.mol^{-1}, $\delta^{44}Ca < -1.5‰$ and higher with variable Li/(Ca+Mg) (see Fig. 11).

iii) Marine burial LMC precipitated in sediment-buffered conditions ($dEQ^{Li} < 0.9$) should preserve the original δ^7Li of primary carbonates. If the original sediment was aragonite (as in the Bahamas), then by using the Li isotope fractionation factor between aragonite and seawater, in theory it could be possible to estimate the δ^7Li of corresponding seawater. However, while modern GBB aragonite sediments have a limited range of δ^7Li ($\Delta^7Li_{carb\text{-}sw} \sim -9\pm1‰$), this is not the case globally, with δ^7Li of modern biogenic aragonite between +15 to +24‰ ($\Delta^7Li_{carb\text{-}sw} \sim -16$ to $-7‰$, Dellinger et al., 2018). Thus, the δ^7Li of ancient LMC formed in sediment-buffered conditions can only be known within ±5‰ uncertainty unless the specific origin of the aragonite is known. Evidence for preservation of the $\delta^{18}O$ of original aragonite sediments would indicate marine burial diagenesis under completely sediment-buffered conditions (for Li isotopes).

iv) Meteoric LMC formed in fluid-buffered conditions ($dEQ^{Li} > 0.9$) may have highly variable Li isotope composition. Meteoric diagenesis, usually characterized by negative $\delta^{13}C$ and $\delta^{18}O$ excursions (Lohman, 1988; Melim and Swart 2001), decreases the Li/(Ca+Mg) ratio to low values of carbonates (0-6 μmol.mol^{-1}) and imparts unpredictable Li isotopic signatures ($\Delta^7Li_{carb\text{-}sw}$ values -15 to $-3‰$) unrelated to the original seawater composition. For many carbonates in the geologic record, this type of alteration can be clearly identified using sedimentological and petrographic evidence (see for instance Hood et al., 2018).

Based on our study of the Bahamas carbonates, we can also make predictions about whether Li isotope excursions measured in platform carbonates correspond to changes in the oceanic δ^7Li or are produced by diagenesis and/or mixing with other types of carbonates (e.g. pelagic LMC). For example, a transition from marine to meteoric fluid-buffered diagenetic LMC (I in Fig. 11) is characterized by lowering and more variable δ^7Li, positive correlations between δ^7Li and $\delta^{13}C$ (and maybe $\delta^{18}O$), no change or slight decreases of the Li/(Ca+Mg), and negative correlation between δ^7Li and Sr/(Ca+Mg). Mixing between marine diagenetic fluid-buffered LMC and pelagic LMC or dolomite (II in Fig. 11) is characterized by a homogeneous δ^7Li, Sr/(Ca+Mg) and $\delta^{13}C$ but variable Li/(Ca+Mg). A transition or mixture between marine fluid-buffered and sediment-buffered diagenetic LMC result in negative correlation between δ^7Li and Li/(Ca+Mg), Sr/(Ca+Mg) and $\delta^{13}C$ (III in Fig. 11). In that case, the correlation between δ^7Li and Sr/(Ca+Mg) is characterized by a significantly less steep slope compared to the transition between fluid-buffered marine and meteoric LMC (Figs. 9 and 11). We also observe that mixing between marine sediment-buffered LMC and pelagic LMC is characterized by a positive correlation between δ^7Li and Li/(Ca+Mg) and negative trends between δ^7Li and Sr/(Ca+Mg) and $\delta^{13}C$ (IV in Fig. 11).

Table 3

Summary of Li isotope and Li/(Ca+Mg) signatures of different diagenetic carbonates and threshold values for other geochemical proxies for recognizing the influence of diagenesis on Li isotopes.

Process	Type of diagenesis	Extent of diagenesis*	Mineralogy	Mean $\Delta^7Li_{carb\text{-}SW}$ (± 1σ)	Range of $\Delta^7Li_{carb\text{-}SW}$	Range of Li/(Ca+Mg) (μmol/mol)	Other geochemical proxies**
Aragonite early diagenesis	Meteoric	Fluid-buffered	LMC	–9±4‰	–15 to –3‰	0-6	• Low $\delta^{13}C$ (0 to -12‰; $dEQ^C > 0.1$) • Low B/Ca (<15 umol/mol; $EQ^B > 0.9$)
	Marine	Fluid-buffered	Dolomite	– 0.5±1.0‰	–1 to +1‰	13-22	• High $\delta^{44/40}Ca$ (> -1.5‰; $dEQ^{Ca} > 0.1$) • Low Sr/Ca (< 1 mmol/mol; $dEQ^{Sr} > 0.9$)
		Fluid-buffered	LMC	– 0.5±1.5‰	–2 to +1‰	2-6	• High $\delta^{44/40}Ca$ (> -1.5‰; $dEQ^{Ca} > 0.1$) • Low Sr/Ca (< 2 mmol/mol; $dEQ^{Sr} > 0.9$) • $\delta^{13}C \sim +2$‰
		Fluid to sediment-buffered	LMC	-	–15 to –1‰	2-20	• Low $\delta^{44/40}Ca$ (< -1.5‰; $dEQ^{Ca} < 0.1$) • High Sr/Ca (Sr/Ca > 2; $dEQ^{Sr} > 0.1$)
		Sediment-buffered	LMC	-	–15 to –8‰	2-20	• Preservation of the original $\delta^{18}O$ ($dEQ^O < 0.1$)
Mixing with pelagic carbonates			LMC foraminifera	–1±1.5‰	–4 to 0‰	12-16	
			LMC bulk	– 6.1±1.3‰	–7 to –4‰	20-40	

* Extent of diagenesis (fluid and sediment buffered) are defined in regard to Li isotope.
** References for $\delta^{13}C$ of meteoric diagenesis are: Lohmann et al., (1988) and Melim et al., (1995) for. For B/Ca of meteoric diagenesis: Stewart et al., (2015). For $\delta^{44/40}Ca$ and $\delta^{13}C$ of marine diagenesis: Higgins et al., (2018) and Ahm et al., (2018). For Sr/Ca of marine diagenesis: Banner and Hanson, (1990) and Ahm et al., (2018). See Banner and Hanson (1990) and equations (3) and (4) for the expression of EQ and dEQ values.

8. Conclusions

We have measured the Li isotopic composition and Li/(Ca+Mg) ratio of carbonate samples from an altered coralline Key Largo Limestone from Florida, and from three cores from the Great Bahamas Banks. Our results show that meteoric diagenesis decreases the Li/(Ca+Mg) ratio of carbonates and changes the δ^7Li value towards values associated with carbonate precipitation from meteoric fluids (+16 to +27‰), consistent with mass balance predictions for open-system meteoric alteration. Thus, meteoric diagenesis imparts large variability and unpredictable isotopic signatures unrelated to the original composition of the carbonates. Considering these results, samples showing signs of meteoric alteration are poor candidates for reconstructing the δ^7Li of past seawater. For many carbonates in the geologic record, such alteration can be clearly identified using sedimentological and petrographic evidence (e.g., Hood et al., 2018). In tandem, based on the data from the Bahamas, we suggest that decreases in the Li/(Ca+Mg) ratio associated with decreases in $\delta^{18}O$ and $\delta^{13}C$ values are likely to indicate diagenetic disturbance to the Li system.

In contrast, during marine burial diagenesis, data from the Clino and Unda cores suggest that the δ^7Li value of carbonates may be completely reset to the composition of marine porewaters with only small variability (+30.5±1.5‰). This process can yield remarkably consistent Li isotope ratios that could, at least under fluid-buffered conditions, reliably record seawater composition at the time of diagenetic alteration, even following dolomitization. The data from ODP Site 1007, however, add a note of caution: marine burial diagenesis under more closed-system conditions (perhaps typical of periplatform settings) may not similarly reset carbonate δ^7Li values, leaving carbonates with an isotopic composition (+24 to +29‰) that is intermediate between their original mineralogic composition (sediment-buffered diagenesis) and seawater (fluid-buffered diagenesis). Fluid vs. sediment buffered diagenetic conditions in marine pore fluids can be distinguished through the use of related proxies (e.g. Sr/Ca, Ca isotopes), which may act as a tool to gauge how we can relate carbonate Li isotope signatures to seawater δ^7Li value in the geologic record. Though many questions remain to be resolved, the results of this study provide some guidelines for interpreting the δ^7Li values in bulk carbonate rocks.

Appendix 1: Mass-balance reactive transport model

This appendix presents the equations used to calculate the composition of diagenetic minerals using a simple mass-balance model of carbonate-water interaction, based on the framework developed in previous studies (e.g. Banner and Hanson, 1990). This model relies on the difference in composition between the original carbonate and the diagenetic fluids, on the partition coefficient between diagenetic carbonates and fluids, and on the extent of water-rock interaction (i.e. water-rock ratio). Following Ahm et al., (2018), we also implement this model within a reactive-transport framework (as developed by Fantle et al., (2010) based on diagenesis mass conservation equations of Berner, 1980) to consider the reaction between a downward advecting fluid and limestone. This model allows the evolution of fluid chemistry and diagenetic conditions along the flow path to be taken into account (Ahm et al., 2018). Note also that our reactive transport equations are similar to the model developed by Pogge von Strandamnn et al. (2014) for Li isotopes. For simplification, we assume constant density of fluid and solid in time and space, constant mass of solid over time (i.e., we assume that all the original limestone is recrystallized), and immobile solid (following Fantle and DePaolo, 2006). Using these assumptions, the change of the Li concentration in limestone ($[\mathrm{Li}]_{\mathrm{solid}}$) over time can be expressed as:

$$\frac{\partial [\mathrm{Li}]_{\mathrm{solid}}}{\partial \mathrm{t}} = -R([\mathrm{Li}]_{\mathrm{solid}} - K^{\mathrm{Li}} \times [\mathrm{Li}]_{\mathrm{fluid}}) \qquad (A1)$$

and for the fluid, the evolution of the Li concentration with time is described by:

$$\frac{\partial [\mathrm{Li}]_{\mathrm{fluid}}}{\partial \mathrm{t}} = D\frac{\partial^2 [\mathrm{Li}]_{\mathrm{fluid}}}{\partial \mathrm{z}^2} - v\frac{\partial [\mathrm{Li}]_{\mathrm{fluid}}}{\partial \mathrm{z}} + RM([\mathrm{Li}]_{\mathrm{solid}} - K^{\mathrm{Li}} \times [\mathrm{Li}]_{\mathrm{fluid}}) \qquad (A2)$$

where $[\mathrm{Li}]_{\mathrm{solid}}$ and $[\mathrm{Li}]_{\mathrm{fluid}}$ respectively are the Li concentrations in the limestone and the fluid (in ppm), R is the reaction rate of the carbonates (in $\mathrm{g.g^{-1}.yr^{-1}}$ or $\%.\mathrm{Myr^{-1}}$), K^{Li} is the distribution coefficient between precipitating carbonate and fluid (see equation below), v is the fluid advection rate (in $\mathrm{m.s^{-1}}$), M is the solid to fluid mass ratio, D the diffusion coefficient (in $\mathrm{cm^2.s^{-1}}$) and z is the vertical spatial dimension of unidirectional flowpath (in m). The Li distribution coefficient between secondary carbonate and fluid (K^{Li}) can be expressed as (Banner and Hanson, 1990):

$$K^{\mathrm{Li}} = \frac{[\mathrm{Li}]_{\mathrm{dcarb}}}{[\mathrm{Li}]_{\mathrm{fluid}}} = Kd^{\mathrm{Li}} \times \frac{[\mathrm{Ca}]_{\mathrm{dcarb}}}{[\mathrm{Ca}]_{\mathrm{fluid}}} \qquad (A3)$$

where $[\mathrm{Li}]_{\mathrm{dcarb}}$ and $[\mathrm{Ca}]_{\mathrm{dcarb}}$ are respectively the Li and Ca concentrations in diagenetic carbonates and $\mathrm{Kd}^{\mathrm{Li}}$ is the partition coefficient of Li between carbonate and fluid. At steady-state (solid and fluid concentration constant over time), and for a constant solid Li concentration over time ($[\mathrm{Li}]_{\mathrm{solid}}$ constant), the solution to equation (2) above can be expressed as (De Paolo, 2006; Fantle, 2010; Pogge von Strandmann et al., 2014):

$$[\mathrm{Li}]_{\mathrm{fluid}}(\mathrm{z}) = \frac{[\mathrm{Li}]_{\mathrm{prim}}}{K^{\mathrm{Li}}} + \left([\mathrm{Li}]_{\mathrm{fluid\,0}} - \frac{[\mathrm{Li}]_{\mathrm{prim}}}{K^{\mathrm{Li}}}\right) e^{-z/L^{Li}} \qquad (A4)$$

The Li concentration in the diagenetic carbonate is then:

$$[\mathrm{Li}]_{\mathrm{dCarb}}(\mathrm{z}) = [\mathrm{Li}]_{\mathrm{prim}} + \left(K^{\mathrm{Li}} \times [\mathrm{Li}]_{\mathrm{fluid\,0}} - [\mathrm{Li}]_{\mathrm{prim}}\right) e^{-z/L^{Li}} \qquad (A5)$$

where $[\mathrm{Li}]_{\mathrm{prim}}$ is the Li concentration in the original limestone. For transformation of aragonite or HM-calcite to LM-calcite, $[\mathrm{Ca}]_{\mathrm{dcarb}} = [\mathrm{Ca}]_{\mathrm{prim}}$ and the calcium concentration in the fluid are constant, so the Li/Ca ratio can be expressed as:

$$\left(\frac{\mathrm{Li}}{\mathrm{Ca}}\right)_{\mathrm{dCarb}}(\mathrm{z}) = \left(\frac{\mathrm{Li}}{\mathrm{Ca}}\right)_{\mathrm{prim}} \left(\mathrm{Kd}^{\mathrm{Li}} \times \left(\frac{\mathrm{Li}}{\mathrm{Ca}}\right)_{\mathrm{fluid\,0}} - \left(\frac{\mathrm{Li}}{\mathrm{Ca}}\right)_{\mathrm{prim}}\right) e^{-\frac{z}{L^{Li}}} \qquad (A6)$$

The term "L^{Li}" is the lithium reactive length scale, and its value depends upon the advection and diffusion rates of the given element:

$$(L^{Li})^{-1} = \left(\frac{v^2}{4D^2} + \frac{RMK^{Li}}{D}\right)^{1/2} - \frac{v}{2D} \quad (A7)$$

For the isotope composition of the fluid, the steady-state expression is:

$$\left(\frac{^7Li}{^6Li}\right)_{\text{fluid}} = \frac{\left(\frac{^7Li}{^6Li}\right)_{\text{prim}}}{\alpha_{prec}^{Li}} \times \frac{[\text{Li}]_{\text{prim}}}{K^{\text{Li}} \times [\text{Li}]_{\text{fluid}}(z)} + \left(\left(\frac{^7Li}{^6Li}\right)_{\text{fluid 0}} \times \frac{[\text{Li}]_{\text{fluid 0}}}{[\text{Li}]_{\text{fluid}}(z)} - \frac{\left(\frac{^7Li}{^6Li}\right)_{\text{prim}}}{\alpha_{prec}^{Li}} \times \frac{[\text{Li}]_{\text{prim}}}{K^{\text{Li}} \times [\text{Li}]_{\text{fluid}}(z)}\right) e^{-\frac{z}{L'}} \quad (A8)$$

With $(^7Li/^6Li)_{fluid}$, $(^7Li/^6Li)_{fluid\ 0}$ and $(^7Li/^6Li)_{prim}$ respectively the Li isotope ratio for the fluid at depth z, for the initial fluid and for the primary carbonates. For the carbonate, we have:

$$\left(\frac{^7Li}{^6Li}\right)_{\text{dcarb}} = \left(\frac{^7Li}{^6Li}\right)_{\text{prim}} \times \frac{[\text{Li}]_{\text{prim}}}{K^{\text{Li}} \times [\text{Li}]_{\text{fluid}}(z)} + \left(\left(\frac{^7Li}{^6Li}\right)_{\text{fluid 0}} \times \frac{\alpha_{prec}^{Li} \times [\text{Li}]_{\text{fluid 0}}}{[\text{Li}]_{\text{fluid}}(z)} - \left(\frac{^7Li}{^6Li}\right)_{\text{prim}} \times \frac{[\text{Li}]_{\text{prim}}}{K^{\text{Li}} \times [\text{Li}]_{\text{fluid}}(z)}\right) e^{-z/L'}$$

(A9)

with 'L' being the reactive length scale of the isotope ^{6}Li:

$$(L')^{-1} = \left(\frac{v^2}{4(\frac{D}{\alpha_{diff}^{Li}})^2} + \frac{RMK^{Li}}{\alpha_{prec}^{Li}(\frac{D}{\alpha_{diff}^{Li}})}\right)^{1/2} - \frac{v}{2\left(\frac{D}{\alpha_{diff}^{Li}}\right)} \quad (A10)$$

The parameters α^{Li}_{prec} and α^{Li}_{diff} are respectively the Li isotope fractionation factors during precipitation of carbonates ($\Delta^{Li}_{carb\text{-}fluid} \sim 1000 \times \ln(\alpha^{Li}_{prec})$) and diffusion in liquid. The depth of the precipitating diagenetic carbonate relative to the reactive length scale exerts a first-order control on the composition of the diagenetic carbonate, in particular influencing whether the carbonate composition is fluid or sediment-buffered (Fantle et al., 2010). According to Eq. (A4), if the diagenetic carbonate precipitates at a much shallower depth than the reactive length scale ($z << L$), then $[Li]_{fluid}(z) = [Li]_{fluid\ 0}$, and $[Li]_{sec}(z) = K^{Li} \times [Li]_{fluid\ 0}$, which means that the composition of the secondary carbonate precipitating at this depth is fluid-buffered. In this case, the Li/Ca ratio of the secondary carbonate minerals is only controlled by the partition coefficient (Kd^{Li}) and the Li/Ca ratio of the infiltrating fluid $(Li/Ca)_{fluid\ 0}$ (Equation 1). However, if $z >> L$, then $[Li]_{fluid}(z) = (K^{Li})^{-1} \times [Li]_{prim}$ and $[Li]_{sec}(z) = [Li]_{prim}$, so the composition of the secondary carbonate precipitating at the depth z is sediment-buffered and has the same composition as the primary carbonate minerals. Hence, the Li/Ca ratio of diagenetic carbonates will be unchanged relative to the primary carbonates. In between these two end-members ($z < L$), the composition of the diagenetic carbonate has intermediate values (Ahm et al., 2018) as represented in Fig. (3C and D) and shown in the supplementary data table.

Appendix 2: Influence of silicate contamination during carbonate leaching

LMC-rich samples

Because Li concentrations in carbonates are very low relative to silicates, it is important to determine the extent to which the δ^7Li and Li/(Ca+Mg) values of carbonate leachates are influenced by dissolution of silicates phases during sample preparation (Vigier et al., 2007, Bastian et al., 2018). To assess this effect, some samples were subjected to a series of different leaching steps (between 2 and 5 leaching steps) in order to evaluate the change in Li/(Ca+Mg) and δ^7Li with increasing dissolution of non-carbonate phases. The leaching tests were done on samples from 1007 (all containing less than 10% dolomite). Two types of leaching tests were done: i) some samples were dissolved twice (two different powder aliquots) with different amounts of acid in order to dissolve about 40% and 80% of the mass of the sample, ii) another set of samples was sequentially dissolved in 4 steps with the dissolution of about 25% each time. In all tests, we used HCl 0.05N. Results are presented in the supplementary data table and presented in Fig. (A1)

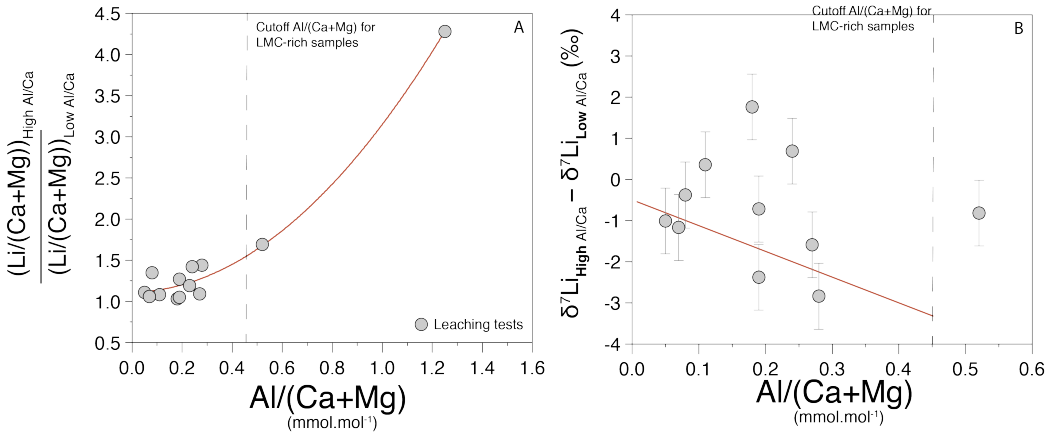

Fig. A1: A) Li isotope difference between the leached fraction having high Al/(Ca+Mg) and that having low Al/(Ca+Mg) ($\delta^7Li_{High\ Al/Ca} - \delta^7Li_{Low\ Al/Ca}$) as a function of Al/(Ca+Mg). B) $(Li/Ca)_{High\ Al/Ca}$ / $(Li/Ca)_{Low\ Al/Ca}$) as a function of Al/(Ca+Mg). By "normalizing" between high and low Al/(Ca+Mg), we just look at the variability in Li/(Ca+Mg) and δ^7Li resulting only from the influence of silicate contamination.

We observe that increasing the amount of carbonate dissolution systematically results in an increase of the Al/(Ca+Mg) and Li/(Ca+Mg), and there is a positive correlation between Li/(Ca+Mg) and Al/(Ca+Mg) (fig. A1). We attribute this relationship to increasing contribution of silicate minerals during dissolution leading to higher Li/(Ca+Mg) and Al/(Ca+Mg) ratios. This result suggests that Li/(Ca+Mg) is particularly sensitive to silicate contamination during leaching, as expected. The results for Li isotopes are not straightforward as some samples show only small change of δ^7Li as a function of Al/(Ca+Mg) while others have decreasing δ^7Li with Al/(Ca+Mg) and more rarely increase of δ^7Li with Al/Ca. Altogether, we observe that at Al/(Ca+Mg) of 0.45 mmol/mol, the ($\delta^7Li_{High\ Al/Ca} - \delta^7Li_{Low\ Al/Ca}$) is –3 to +2‰ offset compared to the $\delta^7Li_{Low\ Al/Ca}$, and the ($(Li/Ca)_{High\ Al/Ca}$ / $(Li/Ca)_{Low\ Al/Ca}$) is higher by a factor of 1.5 for each sample (fig. A1). We consider this Al/(Ca+Mg) value of 0.45 mmol/mol as an upper limit (cutoff value) for LMC-rich samples (or dolomite-poor) because higher Al/(Ca+Mg) samples would have an uncertainty too large due to potential silicate contamination. The great majority of the dolomite-poor samples have Al/(Ca+Mg) < 0.2 mmol/mol and only 2 measured samples (both from the 1007 site) have Al/(Ca+Mg) > 0.45 mmol/mol and are excluded from the discussion. Our cutoff Al/(Ca+Mg) value is about two times lower than in other studies on Li isotopes in carbonates; the studies of Pogge von Strandmann (2013, 2017) on past carbonates used a threshold value of 0.8 mmol/mol, whereas Bastian et al. (2018) suggest an even higher Al/Ca ratio value for leaching ancient (fossil) carbonate material and foraminifera.

Dolomite-rich samples

There is a positive correlation between Al/(Ca+Mg), %wt dolomite and Mg/(Ca+Mg) in Unda and Clino samples from this study (fig. A2). In addition, we observe that the trend defined by these samples is very distinct relative to the trend defined by leaching test of LMC-rich samples described above. Because Clino-Unda dolomite-rich samples contain no or very few non-carbonate phases we interpret these trends reflect a higher proportion of Al in dolomite relative to other carbonate phases (fig.A2). Hence the high Al/(Ca+Mg) of dolomite-rich samples is not indicative of silicate contamination and we do not use the cutoff value of 0.45 mmol/mol for these samples.

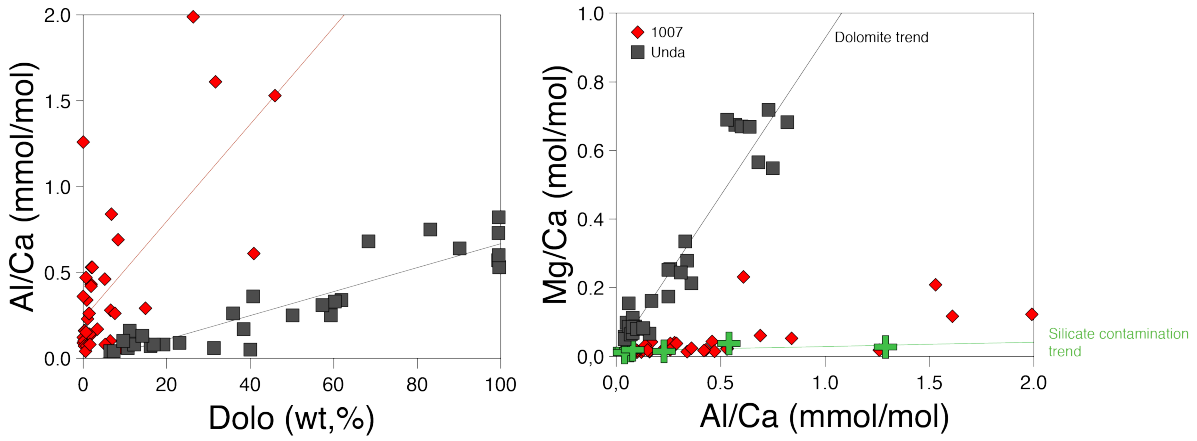

Fig. 2 A) Al/Ca as a function of the proportion of dolomite for 1007 samples and Unda. B) Mg/Ca as a function of Al/Ca, the dolomite trend is represented by Unda. The silicate contamination trend by the leaching tests of LMC-rich samples as described above.

Appendix 3: Calculation of the δ^7Li and Li/Ca ratio of the LMC component

In order to quantify the composition of the LMC component in samples from Site 1007 and from the Clino and Unda cores, and to determine its origin, we use a simple mass balance to correct for aragonite and dolomite composition for each sample assuming a mixture between calcite, aragonite and dolomite:

$$\left(\frac{\mathrm{Li}}{\mathrm{Ca}}\right)_{\mathrm{LMC}}(\mathrm{z}) = \frac{\left(\frac{\mathrm{Li}}{\mathrm{Ca}}\right)_{\mathrm{sample}} - \frac{\mathrm{wt\%_{arag}}}{(\mathrm{wt\%_{arag}} + \mathrm{wt\%_{LMC}} + \mathrm{wt\%_{dol}})} \times \left(\frac{\mathrm{Li}}{\mathrm{Ca}}\right)_{\mathrm{arag}} - \frac{\mathrm{wt\%_{dol}}}{(\mathrm{wt\%_{arag}} + \mathrm{wt\%_{LMC}} + \mathrm{wt\%_{dol}})} \times \left(\frac{\mathrm{Li}}{\mathrm{Ca}}\right)_{\mathrm{dol}}}{\frac{\mathrm{wt\%_{LMC}}}{(\mathrm{wt\%_{arag}} + \mathrm{wt\%_{LMC}} + \mathrm{wt\%_{dol}})}}$$

and

$$\delta^7 Li_{\mathrm{LMC}}(\mathrm{z}) = \frac{\delta^7 Li_{sample} \times \left(\frac{\mathrm{Li}}{\mathrm{Ca}}\right)_{\mathrm{sample}} - \frac{\mathrm{wt\%arag}}{(\mathrm{wt\%arag} + \mathrm{wt\%_{LMC}} + \mathrm{wt\%_{dol}})} \times \delta^7 Li_{arag} \times \left(\frac{\mathrm{Li}}{\mathrm{Ca}}\right)_{\mathrm{arag}} - \frac{\mathrm{wt\%_{dol}}}{(\mathrm{wt\%arag} + \mathrm{wt\%_{LMC}} + \mathrm{wt\%_{dol}})} \times \delta^7 Li_{arag} \times \left(\frac{\mathrm{Li}}{\mathrm{Ca}}\right)_{\mathrm{dol}}}{\frac{\mathrm{wt\%_{LMC}}}{(\mathrm{wt\%arag} + \mathrm{wt\%_{LMC}} + \mathrm{wt\%_{dol}})} \times \left(\frac{\mathrm{Li}}{\mathrm{Ca}}\right)_{\mathrm{LMC}}}$$

We assume a constant Li/Ca of 9.2±1.2 µmol.mol^{-1} and a δ^7Li of 22±1‰ for the aragonite component, a value of Li/Ca of 32±3 µmol.mol^{-1} and δ^7Li of 31±1‰ for dolomite for Clino and Unda Pleistocene sediments (see section 7), and values of 23±1 µmol.mol^{-1} and δ^7Li of 31±1‰ for dolomite for Unda Pliocene sediments. The Li/Ca and δ^7Li of the LMC of each sample can be calculated from the equations above. For three 1007 samples (71.1 mbsf, 78.4 mbsf, 152.3 mbsf) and four Unda samples (between 281.99 and 286.82 mbsf) the calculated uncertainty (±6‰ to ±12‰ for δ^7Li) was too high due to low proportion of LMC (<15%) and therefore these samples are excluded from the figure 8 and from the interpretation. All the data are in the supplementary data table.

Acknowledgements

This work was supported by the American Chemical Society Petroleum Research Fund (award 53418-DNI2 to AJW) and by a COFUND International Junior Research Fellowship awarded to Mathieu Dellinger and held at Durham University. We thank the Associate Editor and three anonymous reviewers for their constructive comments on the manuscript.

References

Ahm, A.-S.C., Bjerrum, C.J., Blättler, C.L., Swart, P.K., Higgins, J.A., 2018, Quantifying early marine diagenesis in shallow-water carbonate sediments: Geochimica et Cosmochimica Acta, v. 236, p. 140-159, https://doi.org/10.1016/j.gca.2018.02.042

Banner, J.L., Hanson, G.N., 1990, Calculation of simultaneous isotopic and trace element variations during water-rock interaction with applications to carbonate diagenesis: Geochimica et Cosmochimica Acta, 54, 3123–3137. https://doi.org/10.1016/0016-7037(90)90128-8

Bastian, L., Vigier, N., Reynaud, S., Kerros, M. E., Revel, M., & Bayon, G., 2018. Lithium Isotope Composition of Marine Biogenic Carbonates and Related Reference Materials. *Geostandards and Geoanalytical Research*, *42*(3), 403-415.

Berner, R. A., 1980. Early diagenesis: a theoretical approach (No. 1). Princeton University Press.

Brand, U., Veizer, J., 1980. Chemical diagenesis of a multicomponent carbonate system - 1. Trace elements. J. Sediment. Petrol. 50, 1219–1236. https://doi.org/10.1306/212F7BB7-2B24-11D7-8648000102C1865D

Brand, U., & Veizer, J. (1981). Chemical diagenesis of a multicomponent carbonate system; 2, Stable isotopes. J. Sediment. Petrol. 50, 1219–1236. 51, 987-997.

Caspard, E., Rudkiewicz, J.-L., Eberli, G.P., Brosse, E., Renard, M., 2004. Massive dolomitization of a Messinian reef in the Great Bahama Bank: a numerical modelling evaluation of Kohout geothermal convection. Geofluids 4, 40–60. https://doi.org/10.1111/j.1468-8123.2004.00071.x

Chan, L.H., Edmond, J.M., Thompson, G., Gillis, K., 1992. Lithium isotopic composition of submarine basalts: implications for the lithium cycle in the oceans. Earth Planet. Sci. Lett. 108, 151–160. https://doi.org/10.1016/0012-821X(92)90067-6

Chen, X., Romaniello, S.J., Herrmann, A.D., Hardisty, D., Gill, B.C., Anbar, A.D., 2018a. Diagenetic effects on uranium isotope fractionation in carbonate sediments from the Bahamas. Geochim. Cosmochim. Acta 237, 294–311. https://doi.org/10.1016/j.gca.2018.06.026

Coogan, L. A., M. J. Yakimoski, and M. Ramsay, 2016. "The Li-content and isotopic composition of altered upper oceanic crust and the hydrothermal carbonate within it." *AGU Fall Meeting Abstracts*.

Day, C.C., Henderson, G.M., 2013. Controls on trace-element partitioning in cave-analogue calcite. Geochim. Cosmochim. Acta 120, 612–627. https://doi.org/10.1016/j.gca.2013.05.044

Darrenougue, N., De Deckker, P., Eggins, S., & Payri, C., 2014. Sea-surface temperature reconstruction from trace elements variations of tropical coralline red algae. Quaternary Science Reviews, *93*, 34-46.

Dellinger, M., Gaillardet, J., Bouchez, J., Calmels, D., Galy, V., Hilton, R. G., ... & France-Lanord, C., 2014. Lithium isotopes in large rivers reveal the cannibalistic nature of modern continental weathering and erosion. Earth and Planetary Science Letters, 401, 359-372.

Dellinger, M., Gaillardet, J., Bouchez, J., Calmels, D., Louvat, P., Dosseto, A., ... & Maurice, L., 2015. Riverine Li isotope fractionation in the Amazon River basin controlled by the weathering regimes. Geochimica et Cosmochimica Acta, *164*, 71-93.

Dellinger, M., West, A. J., Paris, G., Adkins, J. F., von Strandmann, P. A. P., Ullmann, C. V., ... & Corsetti, F. A. (2018). The Li isotope composition of marine biogenic carbonates: Patterns and Mechanisms. Geochimica et Cosmochimica Acta, *236*, 315-335.

DePaolo, D. J., 2006. Isotopic effects in fracture-dominated reactive fluid–rock systems. Geochimica et Cosmochimica Acta, 70(5), 1077-1096.

Eberli, G. P., Swart, P. K., & Malone, M., 1997. Shipboard Scientific Party. The Bahamas Transect: Proceedings of the Ocean Drilling Program, A, Initial Report, (166), 850.

Fantle, M.S., DePaolo, D.J., 2006. Sr isotopes and pore fluid chemistry in carbonate sediment of the Ontong Java Plateau: Calcite recrystallization rates and evidence for a rapid rise in seawater Mg over the last 10 million years. Geochim. Cosmochim. Acta 70, 3883–3904. https://doi.org/10.1016/j.gca.2006.06.009

Fantle, M.S., Maher, K.M., DePaolo, D.J., 2010. Isotopic approaches for quantifying the rates of marine burial diagenesis. Rev. Geophys. 48, RG3002. https://doi.org/10.1029/2009RG000306

Füger, A., Konrad, F., Leis, A., Dietzel, M., & Mavromatis, V. (2019). Effect of growth rate and pH on lithium incorporation in calcite. Geochimica et Cosmochimica Acta, 248, 14-24.

Gaillardet, J., Calmels, D., Romero-Mujalli, G., Zakharova, E., & Hartmann, J., 2018. Global climate control on carbonate weathering intensity. Chemical Geology.

Gill, B.C., Lyons, T.W., Frank, T.D., 2008. Behavior of carbonate-associated sulfate during meteoric diagenesis

and implications for the sulfur isotope paleoproxy. Geochim. Cosmochim. Acta 72, 4699–4711. https://doi.org/10.1016/j.gca.2008.07.001

Ginsburg, R. N. (Ed.). (2001). Subsurface geology of a prograding carbonate platform margin, Great Bahama Bank: results of the Bahamas Drilling Project.

Hall, J.M., Chan, L.-H., 2004. Li/Ca in multiple species of benthic and planktonic foraminifera: thermocline, latitudinal, and glacial-interglacial variation. Geochim. Cosmochim. Acta 68, 529–545. https://doi.org/10.1016/S0016-7037(03)00451-4

Hall, J.M., Chan, L.-H., McDonough, W.F., Turekian, K.K., 2005. Determination of the lithium isotopic composition of planktic foraminifera and its application as a paleo-seawater proxy. Mar. Geol., Ocean Chemistry over the Phanerozoic and its links to Geological Processes 217, 255–265. https://doi.org/10.1016/j.margeo.2004.11.015

Hathorne, E.C., Felis, T., Suzuki, A., Kawahata, H., Cabioch, G., 2013. Lithium in the aragonite skeletons of massive Porites corals: A new tool to reconstruct tropical sea surface temperatures. Paleoceanography 28, 143–152. https://doi.org/10.1029/2012PA002311

Hathorne, E.C., James, R.H., 2006. Temporal record of lithium in seawater: A tracer for silicate weathering? Earth Planet. Sci. Lett. 246, 393–406. https://doi.org/10.1016/j.epsl.2006.04.020

Hardisty, D. S., Lu, Z., Bekker, A., Diamond, C. W., Gill, B. C., Jiang, G., ... & Planavsky, N. J., 2017. Perspectives on Proterozoic surface ocean redox from iodine contents in ancient and recent carbonate. Earth and Planetary Science Letters, 463, 159-170.

Henderson, G.M., Slowey, N.C., Haddad, G.A., 1999. Fluid flow through carbonate platforms: constraints from 234U/238U and Cl– in Bahamas pore-waters. Earth Planet. Sci. Lett. 169, 99–111. https://doi.org/10.1016/S0012-821X(99)00065-5

Higgins, J.A., Blättler, C.L., Lundstrom, E.A., Santiago-Ramos, D.P., Akhtar, A.A., Crüger Ahm, A.-S., Bialik, O., Holmden, C., Bradbury, H., Murray, S.T., Swart, P.K., 2018. Mineralogy, early marine diagenesis, and the chemistry of shallow-water carbonate sediments. Geochim. Cosmochim. Acta 220, 512–534. https://doi.org/10.1016/j.gca.2017.09.046

Huh, Y., Chan, L.-H., Zhang, L., Edmond, J.M., 1998. Lithium and its isotopes in major world rivers: implications for weathering and the oceanic budget. Geochim. Cosmochim. Acta 62, 2039–2051. https://doi.org/10.1016/S0016-7037(98)00126-4

vS Hood, A., Planavsky, N. J., Wallace, M. W., & Wang, X. (2018). The effects of diagenesis on geochemical paleoredox proxies in sedimentary carbonates. *Geochimica et Cosmochimica Acta*, *232*, 265-287.

Jacobsen, S.B., Kaufman, A.J., 1999. The Sr, C and O isotopic evolution of Neoproterozoic seawater. Chem. Geol. 161, 37–57. https://doi.org/10.1016/S0009-2541(99)00080-7

James, N.P., Choquette, P.W., 1984. Diagenesis 9. Limestones - The Meteoric Diagenetic Environment. Geosci. Can. 11.

Kenter, J.A.M., Ginsburg, R.N., Troelstra, S.R., 2001. Sea-level-driven sedimentation patterns on the slope and margin. In: Ginsburg, R.N. (Ed.), Subsurface Geology of a Prograding Carbonate Platform Margin, Great Bahama Bank: Results of the Bahamas Drilling Project. Special Publication. Society of Economic Paleontologists and Mineralogists, Tulsa, OK, pp. 61–100

Kısakűrek, B., James, R.H., Harris, N.B.W., 2005. Li and δ7Li in Himalayan rivers: Proxies for silicate weathering? Earth Planet. Sci. Lett. 237, 387–401. https://doi.org/10.1016/j.epsl.2005.07.019

Lechler, M., Pogge von Strandmann, P.A.E., Jenkyns, H.C., Prosser, G., Parente, M., 2015. Lithium-isotope evidence for enhanced silicate weathering during OAE 1a (Early Aptian Selli event). Earth Planet. Sci. Lett. 432, 210–222. https://doi.org/10.1016/j.epsl.2015.09.052

Liu, X. M., Hardisty, D. S., Lyons, T. W., & Swart, P. K., 2018. Evaluating the fidelity of the cerium paleoredox tracer during variable carbonate diagenesis on the Great Bahamas Bank. Geochimica et Cosmochimica Acta. 248, 25-42.

Lohmann, K., 1988. Geochemical Patterns of Meteoric Diagenetic Systems and Their Application to Studies of Paleokarst, in: Studies in Paleokarst. pp. 58–80. https://doi.org/10.1007/978-1-4612-3748-8_3

Marriott, C.S., Henderson, G.M., Belshaw, N.S., Tudhope, A.W., 2004a. Temperature dependence of δ7Li, δ44Ca and Li/Ca during growth of calcium carbonate. Earth Planet. Sci. Lett. 222, 615–624. https://doi.org/10.1016/j.epsl.2004.02.031

Marriott, C.S., Henderson, G.M., Crompton, R., Staubwasser, M., Shaw, S., 2004b. Effect of mineralogy, salinity, and temperature on Li/Ca and Li isotope composition of calcium carbonate. Chem. Geol., Lithium Isotope Geochemistry 212, 5–15. https://doi.org/10.1016/j.chemgeo.2004.08.002

Melim, L.A., Swart, P.K., Maliva, R.G., 2001. Meteoric and Marine-Burial Diagenesis in the Subsurface of Great Bahama Bank. Subsurface Geology of a Prograding Carbonate Platform Margin, Great Bahama Bank: Results of the Bahamas Drilling Project, Robert N. Ginsburg

Melim, L.A., Swart, P.K., Maliva, R.G., 1995. Meteoric-like fabrics forming in marine waters: Implications for the use of petrography to identify diagenetic environments. Geology 23, 755–758. https://doi.org/10.1130/0091-7613(1995)023<0755:MLFFIM>2.3.CO;2

Millot, R., Vigier, N., Gaillardet, J., 2010. Behaviour of lithium and its isotopes during weathering in the Mackenzie Basin, Canada. Geochim. Cosmochim. Acta 74, 3897–3912. https://doi.org/10.1016/j.gca.2010.04.025

Misra, S., Froelich, P.N., 2012. Lithium isotope history of Cenozoic seawater: changes in silicate weathering and reverse weathering. Science 335, 818–823.

Misra, S., Greaves, M., Owen, R., Kerr, J., Elmore, A. C., & Elderfield, H., 2014. Determination of B/Ca of natural carbonates by HR-ICP-MS. Geochemistry, Geophysics, Geosystems, *15*(4), 1617-1628.

Moore, C.H., Wade, W.J., 2013a. Chapter 8 - Meteoric Diagenetic Environment, in: Moore, C.H., Wade, W.J. (Eds.), Developments in Sedimentology, Carbonate Reservoirs. Elsevier, pp. 165–206. https://doi.org/10.1016/B978-0-444-53831-4.00008-2

Moore, C.H., Wade, W.J., 2013b. Chapter 10 - Burial Diagenetic Environment, in: Moore, C.H., Wade, W.J. (Eds.), Developments in Sedimentology, Carbonate Reservoirs. Elsevier, pp. 239–284. https://doi.org/10.1016/B978-0-444-53831-4.00010-0

Multer H. G., Gischler E., Lundberg J., Simmons K. R. and Shinn E. A. (2002) Key Largo Limestone revisited: Pleistocene shelf- edge facies, Florida Keys, USA. Facies 46, 229–272.

Pogge von Strandmann, P.A.E., Desrochers, A., Murphy, M.J., Finlay, A.J., Selby, D., Lenton, T.M., 2017. Global climate stabilisation by chemical weathering during the Hirnantian glaciation. Geochem. Perspect. Lett. 230–237. https://doi.org/10.7185/geochemlet.1726

Pogge von Strandmann, P.A.E., Jenkyns, H.C., Woodfine, R.G., 2013. Lithium isotope evidence for enhanced weathering during Oceanic Anoxic Event 2. Nat. Geosci. 6, 668–672. https://doi.org/10.1038/ngeo1875

Pogge von Strandmann, P.A.E., Porcelli, D., James, R.H., van Calsteren, P., Schaefer, B., Cartwright, I., Reynolds, B.C., Burton, K.W., 2014. Chemical weathering processes in the Great Artesian Basin: Evidence from lithium and silicon isotopes. Earth Planet. Sci. Lett. 406, 24–36. https://doi.org/10.1016/j.epsl.2014.09.014

Pogge von Strandmann, Philip A. E., Vaks, A., Bar-Matthews, M., Ayalon, A., Jacob, E., Henderson, G.M., 2017. Lithium isotopes in speleothems: Temperature-controlled variation in silicate weathering during glacial cycles. Earth Planet. Sci. Lett. 469, 64–74. https://doi.org/10.1016/j.epsl.2017.04.014

Pogge von Strandmann, P. A. P., Schmidt, D. N., Planavsky, N. J., Wei, G., Todd, C. L., & Baumann, K. H., 2019. Assessing bulk carbonates as archives for seawater Li isotope ratios. Chemical Geology, 530, 119338.

Reijmer, J.J.G., Swart, P.K., Bauch, T., Otto, R., Reuning, L., Roth, S., Zechel, S., 2009. A Re-Evaluation of Facies on Great Bahama Bank I: New Facies Maps of Western Great Bahama Bank, in: Swart, P.K., Eberli, G.P., McKenzie, J.A., Editor, I.J.S., Co-Editor, T.S.S. (Eds.), Perspectives in Carbonate Geology. John Wiley & Sons, Ltd, pp. 29–46. https://doi.org/10.1002/9781444312065.ch3

Roberts, J., Kaczmarek, K., Langer, G., Skinner, L. C., Bijma, J., Bradbury, H., ... & Misra, S. (2018). Lithium isotopic composition of benthic foraminifera: A new proxy for paleo-pH reconstruction. *Geochimica et Cosmochimica Acta*, *236*, 336-350. https://doi.org/10.1016/j.gca.2018.02.038

Rollion-Bard, C., Vigier, N., Meibom, A., Blamart, D., Reynaud, S., Rodolfo-Metalpa, R., Martin, S., Gattuso, J.-P., 2009. Effect of environmental conditions and skeletal ultrastructure on the Li isotopic composition of scleractinian corals. Earth Planet. Sci. Lett. 286, 63–70. https://doi.org/10.1016/j.epsl.2009.06.015

Sauzéat, L., Rudnick, R.L., Chauvel, C., Garçon, M., Tang, M., 2015. New perspectives on the Li isotopic composition of the upper continental crust and its weathering signature. Earth Planet. Sci. Lett. 428, 181–192. https://doi.org/10.1016/j.epsl.2015.07.032

Schlager, W., James, N.P., 1978. Low-magnesian calcite limestones forming at the deep-sea floor, Tongue of the

Ocean, Bahamas. Sedimentology 25, 675–702. https://doi.org/10.1111/j.1365-3091.1978.tb00325.x
Schlager, W. Carbonate sedimentology and sequence stratigraphy (No. 8), 2005. SEPM Soc for Sed Geology.
Scholz, F., Hensen, C., De Lange, G.J., Haeckel, M., Liebetrau, V., Meixner, A., Reitz, A., Romer, R.L., 2010. Lithium isotope geochemistry of marine pore waters – Insights from cold seep fluids. Geochim. Cosmochim. Acta 74, 3459–3475. https://doi.org/10.1016/j.gca.2010.03.026
Stewart, J.A., Gutjahr, M., Pearce, F., Swart, P.K., Foster, G.L., 2015. Boron during meteoric diagenesis and its potential implications for Marinoan snowball Earth δ11B-pH excursions. Geology G36652.1. https://doi.org/10.1130/G36652.1
Swart, P.K., 2015. The geochemistry of carbonate diagenesis: The past, present and future. Sedimentology 62, 1233–1304. https://doi.org/10.1111/sed.12205
Swart, P.K., 2008. Global synchronous changes in the carbon isotopic composition of carbonate sediments unrelated to changes in the global carbon cycle. Proc. Natl. Acad. Sci. 105, 13741–13745. https://doi.org/10.1073/pnas.0802841105
Swart, P.K., Eberli, G., 2005. The nature of the δ13C of periplatform sediments: Implications for stratigraphy and the global carbon cycle. Sediment. Geol., Sedimentology in the 21st Century - A Tribute to Wolfgang Schlager 175, 115–129. https://doi.org/10.1016/j.sedgeo.2004.12.029
Swart, P.K., Melim, L.A., 2000. The Origin of Dolomites in Tertiary Sediments from the Margin of Great Bahama Bank. J. Sediment. Res. 70, 738–748. https://doi.org/10.1306/2DC40934-0E47-11D7-8643000102C1865D
Swart, P.K., Oehlert, A.M., 2018. Revised interpretations of stable C and O patterns in carbonate rocks resulting from meteoric diagenesis. Sediment. Geol. 364, 14–23. https://doi.org/10.1016/j.sedgeo.2017.12.005
Taylor, H.L., Kell Duivestein, I.J., Farkaš, J., Dietzel, M., Dosseto, A., 2018. Lithium isotopes in dolostone as a palaeo-environmental proxy – An experimental approach. Clim. Past Discuss. 1–32. https://doi.org/10.5194/cp-2018-113
Teng, F.-Z., McDonough, W.F., Rudnick, R.L., Dalpé, C., Tomascak, P.B., Chappell, B.W., Gao, S., 2004. Lithium isotopic composition and concentration of the upper continental crust. Geochim. Cosmochim. Acta 68, 4167–4178. https://doi.org/10.1016/j.gca.2004.03.031
Ullmann, C.V., Campbell, H.J., Frei, R., Hesselbo, S.P., Pogge von Strandmann, P.A.E., Korte, C., 2013. Partial diagenetic overprint of Late Jurassic belemnites from New Zealand: Implications for the preservation potential of δ7Li values in calcite fossils. Geochim. Cosmochim. Acta 120, 80–96. https://doi.org/10.1016/j.gca.2013.06.029
Whitaker, F.F., Smart, P.L., 2007. Geochemistry of meteoric diagenesis in carbonate islands of the northern Bahamas: 2. Geochemical modelling and budgeting of diagenesis. Hydrol. Process. 21, 967–982. https://doi.org/10.1002/hyp.6533
Zhang, S., Henehan, M. J., Hull, P. M., Reid, R. P., Hardisty, D. S., vS Hood, A., & Planavsky, N. J., 2017. Investigating controls on boron isotope ratios in shallow marine carbonates. Earth and Planetary Science Letters, 458, 380-393.

Table 2: Li isotope, Li/Ca and other trace elements ratios in the Clino and Unda cores, Key Largo Limestone and ODP Site 1007

Core	Name	Depth (m)	δ^7Li (‰)	Li/Ca (µmol/mol)	Mg/Ca (mol/mol)	Al/Ca (mmol/mol)	Mn/Ca (µmol/mol)	Fe/Ca (µmol/mol)	Sr/Ca (mmol/mol)
Clino	Clino 70'6"	21.49	17.7	5.93	0.0070	0.11	1.8	55.6	5.77
Clino	Clino 83'	25.3	24.0	5.41	0.0124	0.07	3.5	70.0	4.26
Clino	Clino 90'	27.43	16.1	2.87	0.0111	0.13	2.0	49.5	2.02
Clino	Clino 103'6"(a)	31.55	25.8						
Clino	Clino 112' (a)	34.19	20.4	4.85	0.0155	0.07	5.3	66.3	3.31
Clino	Clino 123'5"	37.62	21.9	5.92	0.0209	0.08	5.3	90.8	2.45
Clino	Clino 133' (a)	40.54	21.1	5.48	0.0135	0.10	4.2	134.2	2.27
Clino	Clino 192'7"	56.92	21.3	4.68	0.0165	0.15	6.7	153.8	1.71
Clino	Clino 211'8"	64.52	25.2	5.49	0.0186	0.06	3.8	92.7	1.42
Clino	Clino 244'11"	74.65	20.0	6.72	0.0145	0.21	11.2	206.6	1.87
Clino	Clino 252'2"	76.86	25.1	3.91	0.0166	0.05	10.2	93.9	1.49
Clino	Clino 277'.7"	84.61		3.78	0.0163	0.12	7.9	70.4	1.73
Clino	Clino 294'5"	89.74	23.7	5.44	0.0162	0.13	7.4	150.0	1.60
Clino	Clino 318'	96.93	24.8	4.11	0.0184	0.09	9.0	112.9	1.26
Clino	Clino 340'6"	103.78	17.1	4.07	0.0001	0.04	1.4	2.4	2.64
Clino	Clino 366'	111.56		0.94	0.0157	0.03	7.0	33.4	3.14
Clino	Clino 432'	131.67	26.8	1.85	0.0274	0.02	10.2	21.4	1.87
Clino	Clino 483'6"	147.37	28.0	5.26	0.0305	0.03	14.1	24.1	3.44
Clino	Clino 503'8"	155.55	30.5	6.79	0.0580	0.05	13.4	18.0	2.43
Clino	Clino 532'	162.15	31.2	5.61	0.0647	0.03	11.9	13.1	1.39
Clino	Clino 575'3"	175.34	30.3	6.44	0.0517	0.03	15.1	6.5	1.73
Clino	Clino 608'5"	185.45	30.2	9.77	0.0758	0.07	15.5	7.7	2.24
Clino	Clino 736'1"	224.36	24.6	8.52	0.0310	0.34	4.5	29.9	4.60
Clino	Clino 764'3.5"	232.96	24.3	6.10	0.0264	0.20	2.8	21.3	5.27
Clino	Clino 828'1"	252.4	30.5	8.40	0.0636	0.08	16.0	18.1	1.57
Unda	Unda 296'5"	90.4494	21.1	5.07	0.0141	0.24	8.4	158.5	1.68
Unda	Unda 309'5"	94.31	25.6	3.94	0.0175	0.19	12.1	115.1	1.94
Unda	Unda 313'	95.4	22.5	3.61	0.0190	0.19	8.0	126.7	1.55
Unda	Unda 321'5"	97.97	23.8	3.44	0.0186	0.14	16.1	146.8	1.92
Unda	Unda 343'5"	104.67	27.6	2.89	0.0182	0.08	23.4	71.1	1.93
Unda	Unda 350'6"	106.83	27.3	2.69	0.0231	0.10	30.7	85.2	2.39
Unda	Unda 359'2"	109.47	30.8	28.98	0.5479	0.75	26.7	424.4	1.33
Unda	Unda 360'	109.73	29.4	13.39	0.2131	0.36	17.0	161.5	1.77
Unda	Unda 369'1"	112.5	29.6	5.61	0.0574	0.04	15.9	94.6	2.29
Unda	Unda 377'2"	114.96	28.9	10.18	0.0977	0.05	11.9	106.3	1.98
Unda	Unda 386'1"	117.68	30.3	15.36	0.1609	0.17	13.9	144.2	1.98
Unda	Unda 396'6"	120.85	30.2	17.42	0.1553	0.06	11.6	132.6	2.45
Unda	Unda 403'73	123.01	30.7	14.13	0.1120	0.08	9.8	69.9	2.27
Unda	Unda 411'4"	125.37	30.4	14.20	0.1739	0.25	13.6	68.3	1.46
Unda	Unda 428'10"	130.71	30.8	12.61	0.0865	0.06	14.6	36.9	1.73
Unda	Unda 433'10"	132.23	30.2	10.75	0.0504	0.04	14.9	27.2	1.89
Unda	Unda 442'1"	134.75		9.80	0.0641	0.07	16.8	38.8	1.48
Unda	Unda 450'6"	137.31	31.2	9.22	0.0679	0.08	16.5	18.4	1.39
Unda	Unda 458'8"	139.8	30.2	10.36	0.0665	0.16	12.1	21.9	1.92
Unda	Unda 466'10"	142.29	30.7	9.53	0.0866	0.09	28.6	16.6	1.56
Unda	Unda 476'4"	145.19	30.7	8.24	0.0858	0.08	9.4	16.7	1.68
Unda	Unda 485'8"	148.03	30.6	7.95	0.0799	0.10	9.0	18.2	1.68
Unda	Unda 493'2"	150.32		8.77	0.0823	0.13	9.3	16.5	1.61
Unda	Unda 901'	274.62	30.4	18.23	0.2778	0.34	29.0	109.0	0.62
Unda	Unda 904'4"	275.64	30.5	16.43	0.2546	0.26	23.3	81.3	0.62
Unda	Unda 910'	277.37	30.8	16.76	0.2525	0.25	23.5	99.6	0.61
Unda	Unda 915'10"	279.15	30.8	18.77	0.3348	0.33	23.6	58.0	0.64
Unda	Unda 920'	280.42	29.9	17.02	0.2443	0.31	19.2	79.0	0.61
Unda	Unda 925'2"	281.99	30.7	24.95	0.6743	0.57	29.9	87.3	0.50
Unda	Unda 931'5"	283.9	30.8	23.60	0.6885	0.53	28.1	96.3	0.50
Unda	Unda 936'9"	285.52	30.6	22.92	0.6697	0.60	28.8	115.4	0.48
Unda	Unda 941'	286.82	30.7	22.97	0.6688	0.64	28.3	97.6	0.48
Unda	Unda 944'8"	287.93	30.7	21.23	0.5647	0.68	28.6	83.5	0.55
Unda	Unda 950'2"	289.61	31.0	23.42	0.6825	0.82	35.0	117.3	0.46
Unda	Unda 955'2"	291.13	30.4	23.54	0.7177	0.73	36.6	137.0	0.42

Core	Name	Depth (m)	δ^7Li (‰)	Li/Ca (µmol/mol)	Mg/Ca (mol/mol)	Al/Ca (mmol/mol)	Mn/Ca (µmol/mol)	Fe/Ca (µmol/mol)	Sr/Ca (mmol/mol)
KL1	KL 1-1	0.04	20.6	1.16	0.0041		1.7		2.15
KL1	KL 1-2	0.022	20.4						
KL1	KL 1-3	0.005	18.7	0.79	0.0029		0.2		1.69
KL1	KL 1-4	-0.015	17.5	5.15	0.0034		0.1		7.09
KL1	KL 1-6	-0.043	17.6	5.64	0.0035		0.2		7.30
KL11	KL 11-3	0.057		0.98	0.0035	0.01	1.0	4.6	2.58
KL11	KL 11-4	0.049		1.41	0.0035	0.02	0.9	6.5	4.84
KL11	KL 11-5	0.0405		0.28	0.0042	0.01	1.7	22.4	4.94
KL11	KL 11-6	0.033		2.06	0.0044	0.00	0.9	4.4	5.13
KL11	KL 11-8	0.015		1.42	0.0044	0.02	0.8	6.0	5.47
KL11	KL 11-12	-0.0215	19.1	6.50	0.0034	0.00	0.6	5.0	9.02
KL11	KL 11-14	-0.037		6.01	0.0037	0.02	1.0	7.5	8.80
KL12	KL 12-1	0.0575		0.54	0.0035	0.02	0.6	4.0	2.18
KL12	KL 12-2	0.049	15.0	0.84	0.0029	0.04	0.0	0.0	2.04
KL12	KL 12-3	0.0405		3.41	0.0029	0.02	0.4	4.2	1.66
KL12	KL 12-4	0.032		1.93	0.0037	0.01	0.5	6.0	2.08
KL12	KL 12-5	0.023	16.9	1.05	0.0036	0.02	0.6	4.4	2.09
KL12	KL 12-6	0.014		5.99	0.0032	0.02	0.5	4.3	2.63
KL12	KL 12-7	0.006	17.2	0.68	0.0030	0.01	0.6	5.5	2.45
KL12	KL 12-8	-0.0065	18.3	5.80	0.0036	0.03	0.5	5.2	9.10
KL12	KL 12-9	-0.0165		5.94	0.0038	0.05	0.7	12.8	9.01
KL12	KL 12-10	-0.0245	17.9	4.87	0.0037	0.01	0.4	3.1	8.94

1194

Leg	Site	Hole	Core	Type	Sec	Upp	Low	Anal	Depth(mbsf)	δ^7Li (‰)	Li/Ca (µmol/mol)	Mg/Ca (mol/mol)	Al/Ca (mmol/mol)	Mn/Ca (µmol/mol)	Sr/Ca (mmol/mol)
166	1007	B	3	H	4	39	40	XRD	23.9	24.4	10.24	0.0133	0.09	17.9	8.68
166	1007	B	5	H	2	39	40	XRD	41.9	26.6	12.20	0.0140	0.16	91.9	7.72
166	1007	B	5	H	4	39	40	XRD	44.9	25.0	14.99	0.0184	1.26	269.2	3.31
166	1007	B	7	H	6	39	40	XRD	65.4	25.6	11.45	0.0156	0.16	72.9	8.11
166	1007	B	8	H	2	39	40	XRD	68.9	23.4	11.24	0.0115	0.12	10.8	10.80
166	1007	B	8	H	4	39	40	XRD	71.9	23.9	9.19	0.0123	0.10	9.8	9.88
166	1007	B	9	H	2	39	40	XRD	78.4	27.4	10.57	0.0097	0.07	2.7	10.40
166	1007	B	11	X	2	39	40	XRD	93.6	23.3	8.72	0.0066	0.07	5.6	10.05
166	1007	B	11	X	4	39	40	XRD	96.6	27.9	15.23	0.0432	0.46	88.1	3.35
166	1007	B	12	X	1	64	65	XRD	101.8	26.0	10.42	0.0179	0.13	7.7	8.83
166	1007	B	13	X	CC	40	41	XRD	111	22.6	9.20	0.0183	0.04	10.4	7.86
166	1007	B	16	X	2	39	40	XRD	140.4		8.99	0.0228	0.23	79.3	7.63
166	1007	B	17	X	2	39	40	XRD	149.3	26.4	9.71	0.0207	0.26	54.8	1.82
166	1007	B	17	X	4	39	40	XRD	152.3	26.6	11.53	0.0424	0.17	6.3	8.76
166	1007	B	23	X	6	39	40	XRD	211	25.7	15.41	0.0401	0.28	188.4	1.70
166	1007	B	24	X	4	39	40	XRD	217.3		21.36	0.0381	0.26	150.5	1.83
166	1007	B	25	X	4	39	40	XRD	226.4	28.4	11.46	0.0163	0.05	305.1	1.93
166	1007	B	26	X	4	39	40	XRD	235.5	28.4					
166	1007	B	28	X	2	39	40	XRD	251	28.1	10.18	0.0174	0.10	201.9	1.43
166	1007	B	34	X	1	62	63	XRD	304.9	28.9	13.79	0.0315	0.14	114.2	1.84
166	1007	B	36	X	1	14	15	XRD	322.9	29.0	7.97	0.0276	0.08	49.3	1.77
166	1007	B	38	X	1	13	14	XRD	341.2	27.3	6.10	0.0107	0.08	45.1	1.27
166	1007	B	39	X	1	36	37	XRD	350.6	26.1	13.27	0.0238	0.53	37.0	2.54
166	1007	B	41	X	CC	27	28	XRD	368.8	24.6	10.17	0.0177	0.15	70.9	8.25
166	1007	C	21	R	3	43	44	XRD	497.6	23.6	10.56	0.0206	0.53	159.2	3.69
166	1007	C	23	R	1	43	44	XRD	514.1	23.1	14.78	0.0130	0.34	106.8	4.58
166	1007	C	23	R	5	39	40	XRD	518.9	24.2	16.62	0.0185	0.43	59.7	3.43
166	1007	C	23	R	7	40	41	XRD	521.3		13.83	0.0149	0.47	89.2	4.31
166	1007	C	24	R	3	40	41	XRD	526.5	22.7	13.35	0.0168	0.42	63.5	3.80
166	1007	C	25	R	1	45	46	XRD	533.4	29.5	8.43	0.0188	0.26	73.7	3.16
166	1007	C	38	R	3	38	39	XRD	661	23.3	36.37	0.1218	1.99	14.3	4.57
166	1007	C	41	R	3	40	41	XRD	689.7	22.6	20.89	0.0521	0.84	12.7	3.88
166	1007	C	41	R	5	40	41	XRD	692.7	24.7	13.29	0.0236	0.36	57.8	4.68
166	1007	C	43	R	3	40	41	XRD	709.3	22.2	22.73	0.2325	0.61	24.3	3.79
166	1007	C	44	R	1	40	41	XRD	716	23.2	19.87	0.0610	0.69	8.7	4.03
166	1007	C	45	R	5	40	41	XRD	731.3	23.4	37.53	0.1167	1.61	16.5	5.68
166	1007	C	46	R	1	41	42	XRD	735.2	24.7					
166	1007	C	47	R	3	39	40	XRD	747.5	22.7	30.22	0.2083	1.53	69.5	3.76
166	1007	C	48	R	5	37	38	XRD	759.6	26.0	12.90	0.0366	0.29	58.4	3.79

1195